X-ray Flares from Sgr A* (Galactic center)

(Baganoff et al. 2001)

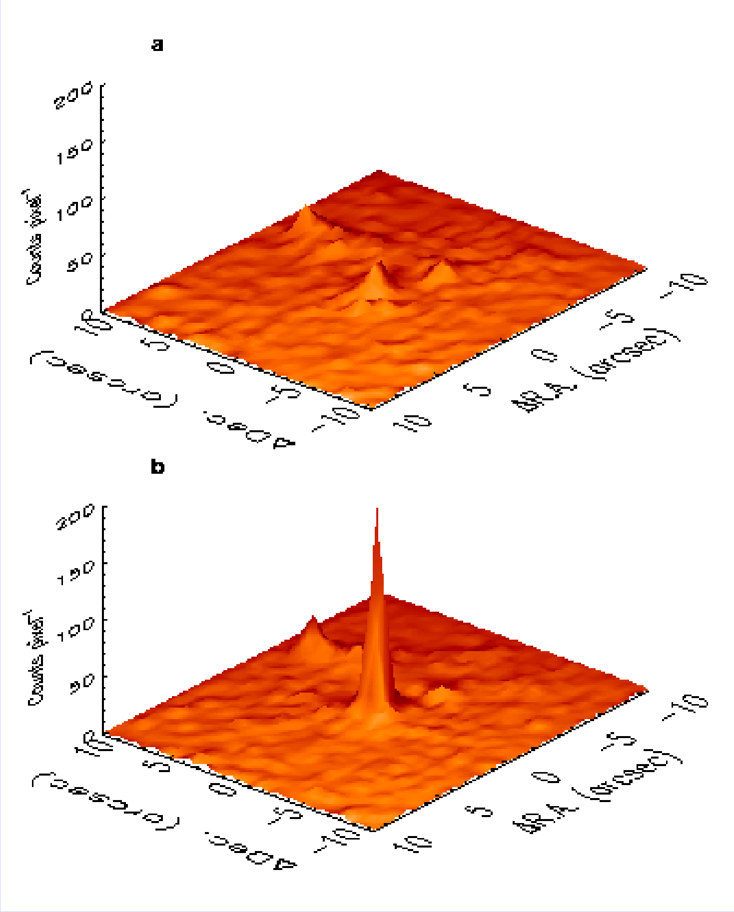

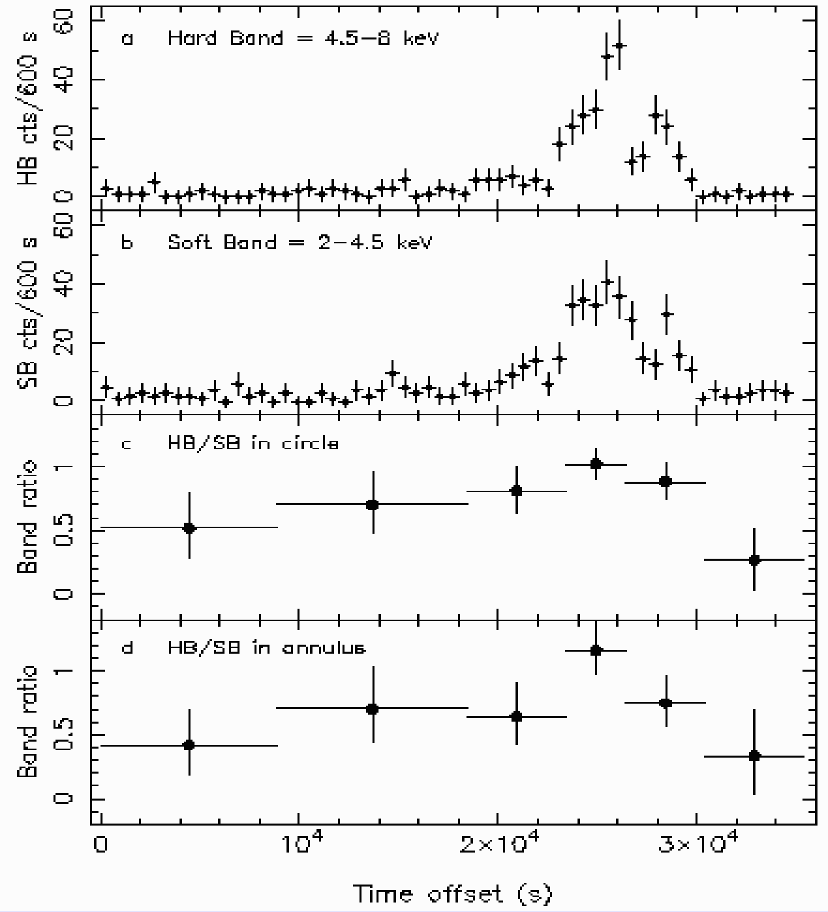

During a flare, Sgr A*'s X-ray luminosity can increase by more than one order of magnitude.

This X-ray flare lasted for a few hours. Significant variation in flux was observed over 10 minutes.

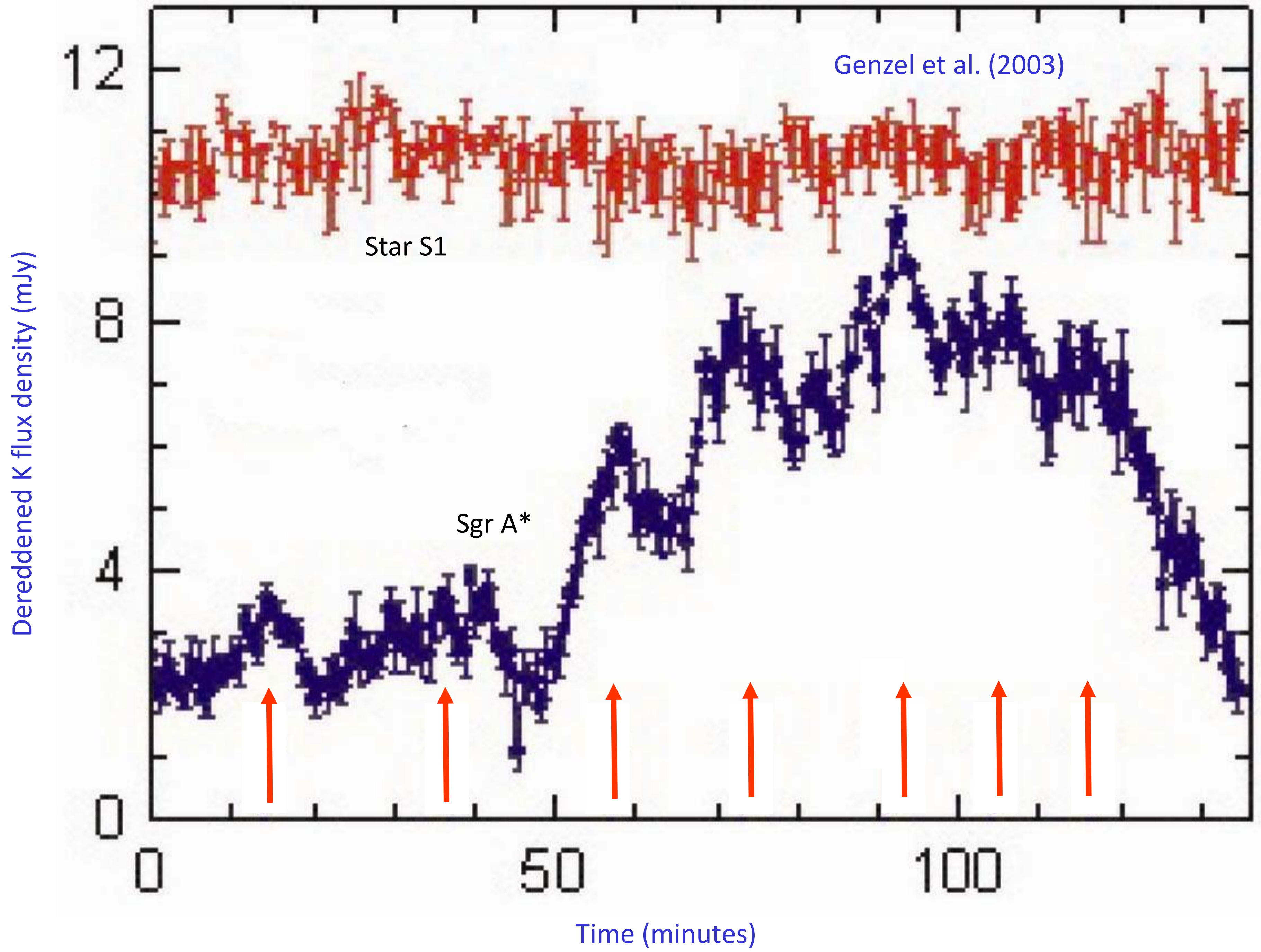
Genzel et al. (2003)
Star S1
Sgr A*
Dereddened K flux density (mJy)
Time (minutes)
0
4
8
12
0
50
100

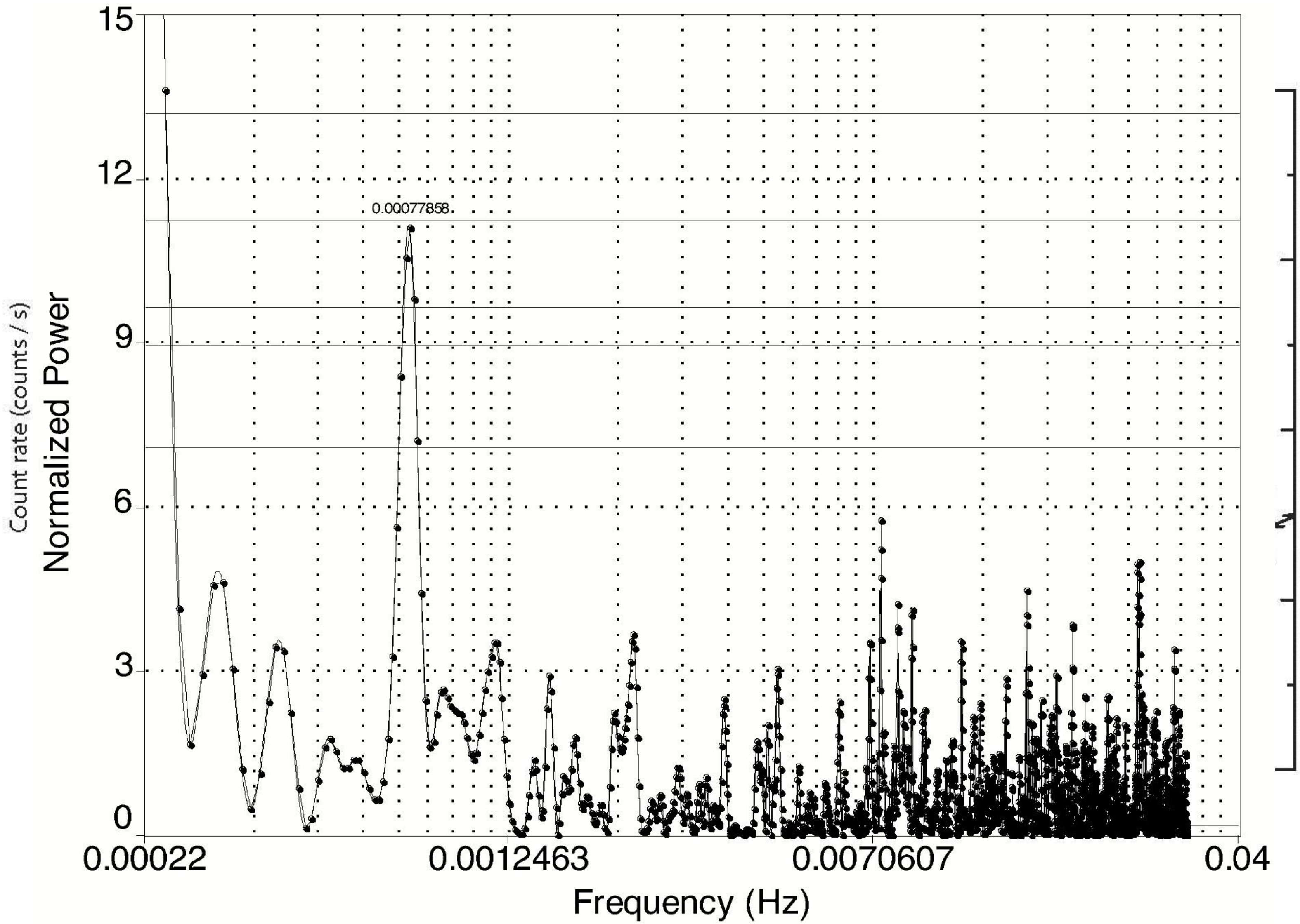

(Belanger, Goldwurm, Melia et al. 2005)

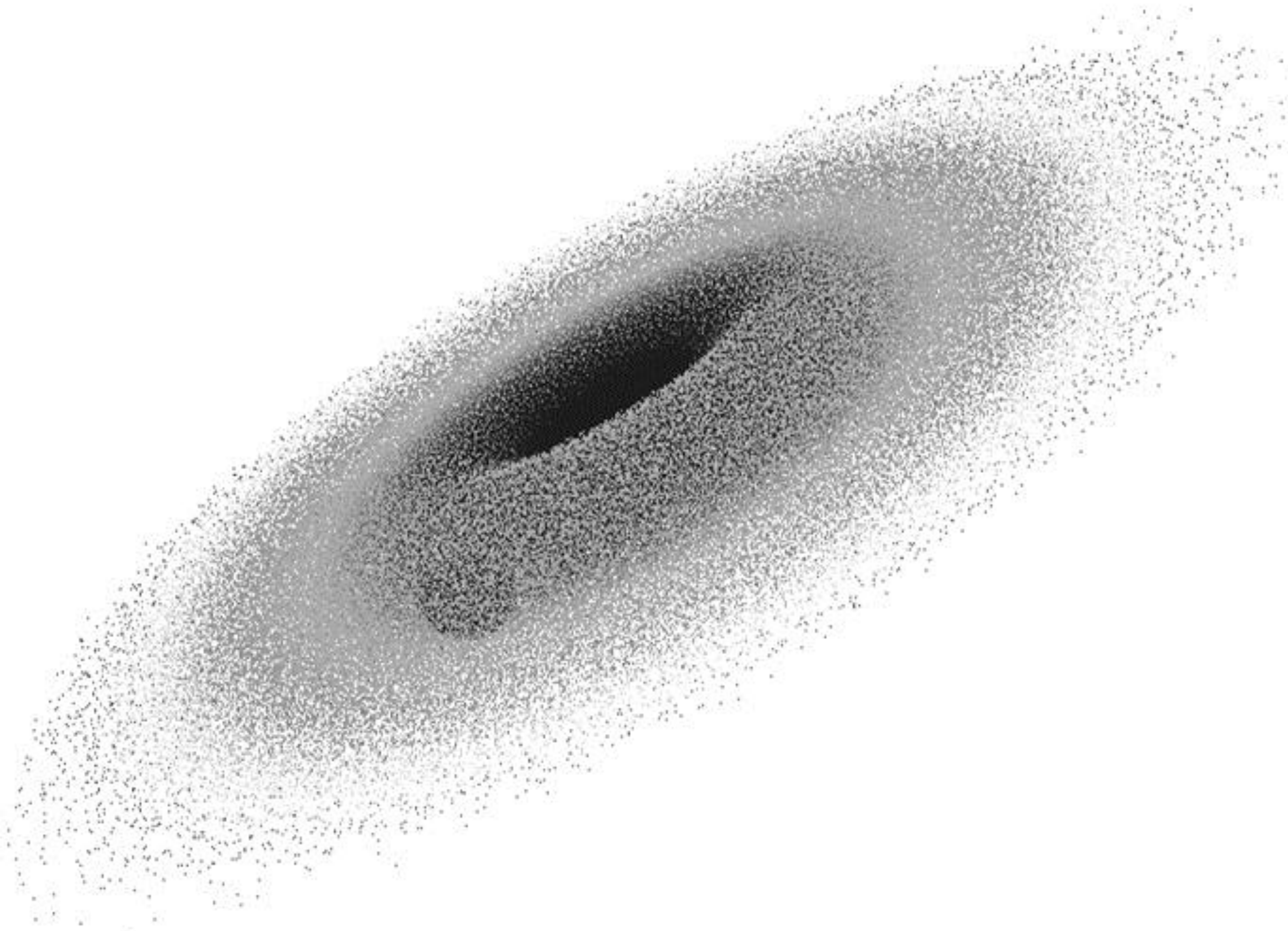

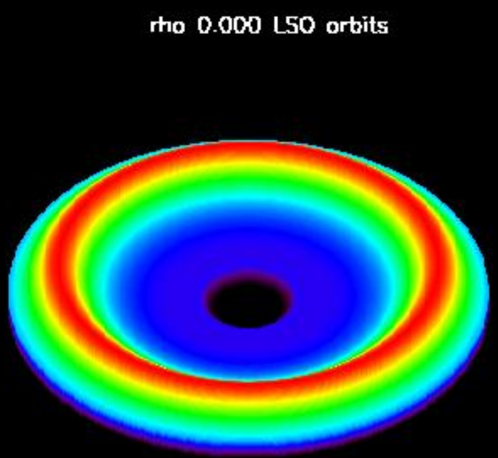

Tagger and Melia (2006)

The Relativistic Particle Distribution

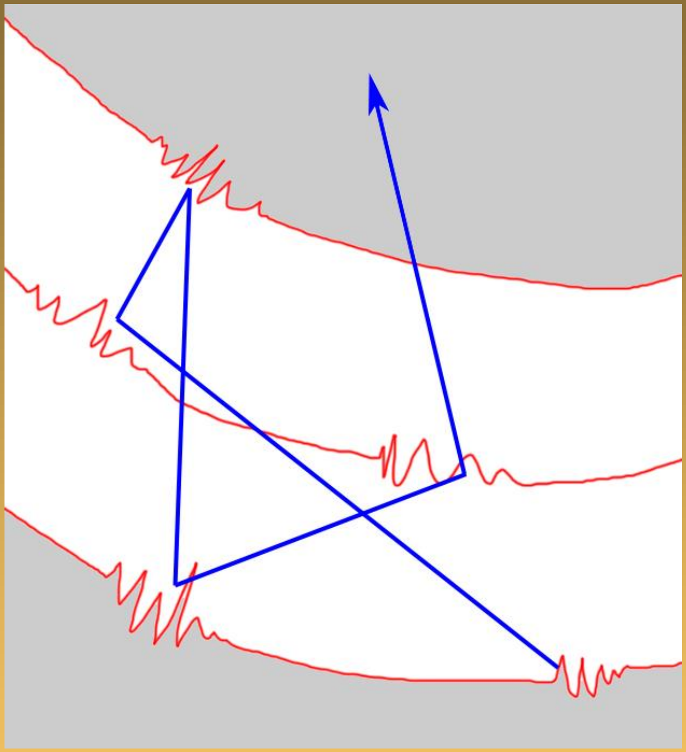

The instability creates a turbulent medium and magnetic field, and some particles “bounce” off the turbulent fluctuations and gain energy (via the “second-order” Fermi process). A fraction of the plasma thereby becomes relativistic and unbounded, escaping outwards perpendicular to the disk.

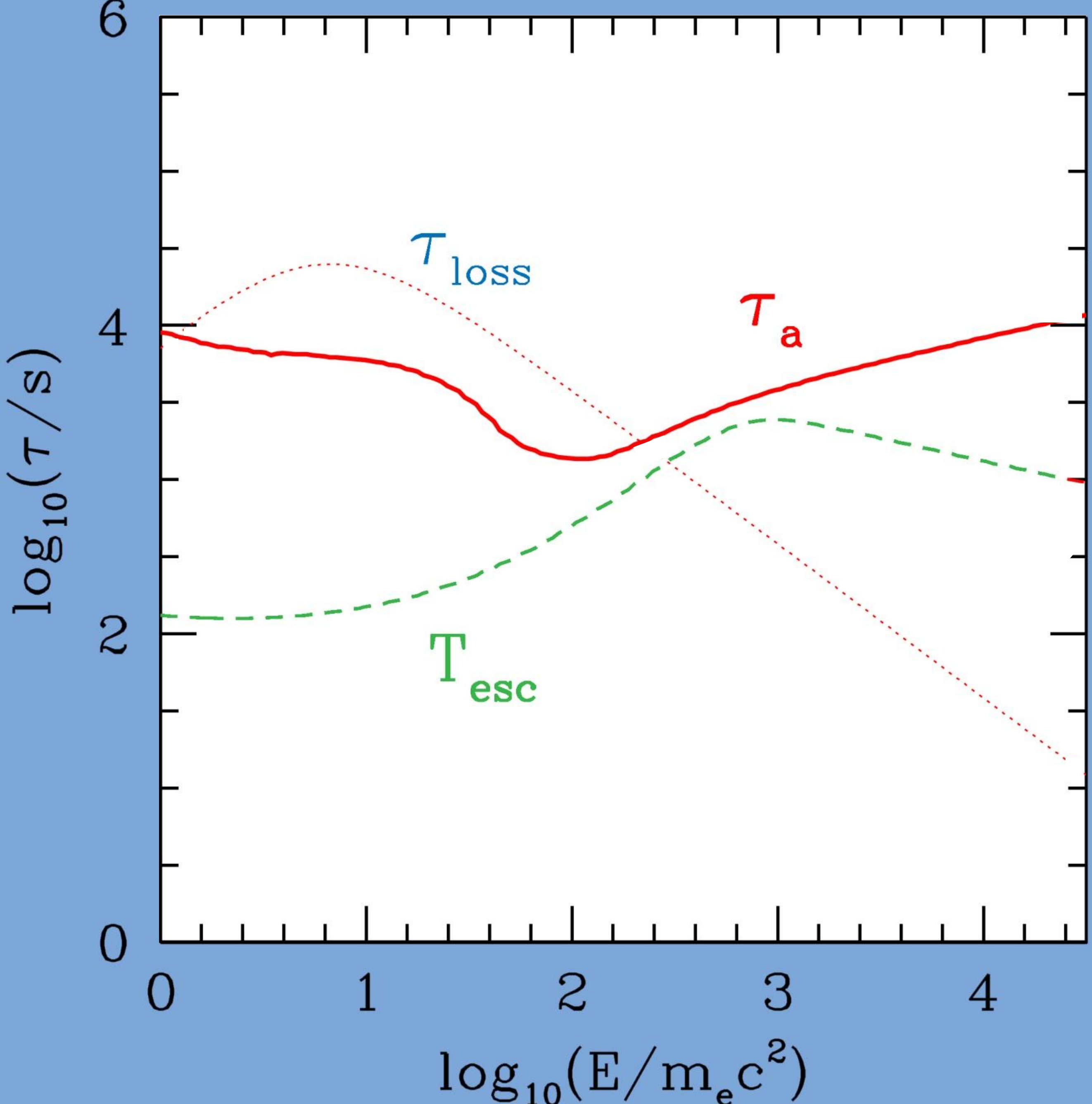

6
4
2
0
0
1
2
3
4
$\log_{10}(\tau/s)$
$\log_{10}(E/m_e c^2)$
τ_{loss}
τ_a
T_{esc}

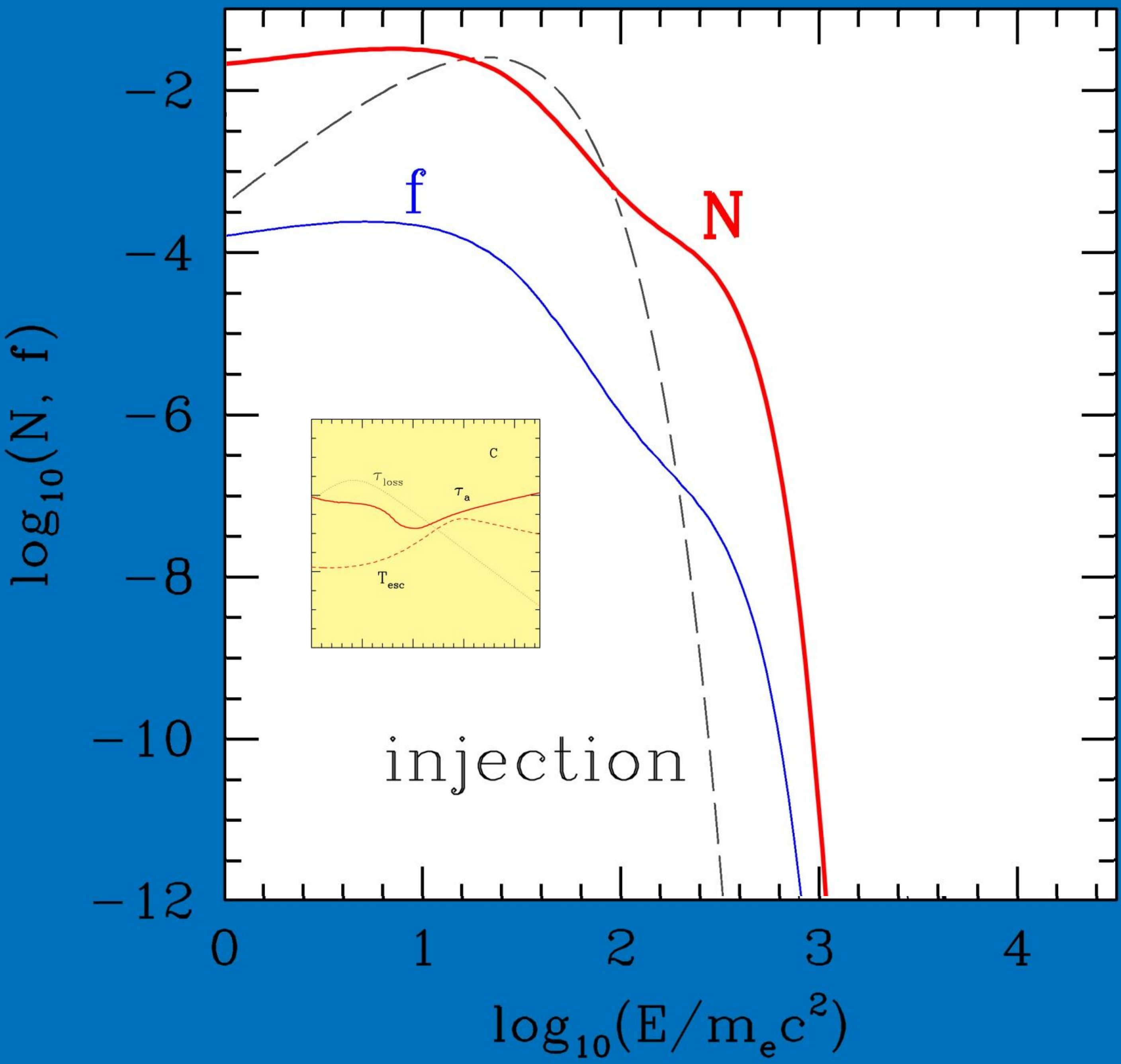

-2
-4
-6
-8
-10
-12
0
1
2
3
4
$\log_{10}(N,\ f)$
$\log_{10}(E/m_e c^2)$
f
N
injection
C
τ_{loss}
τ_a
T_{esc}

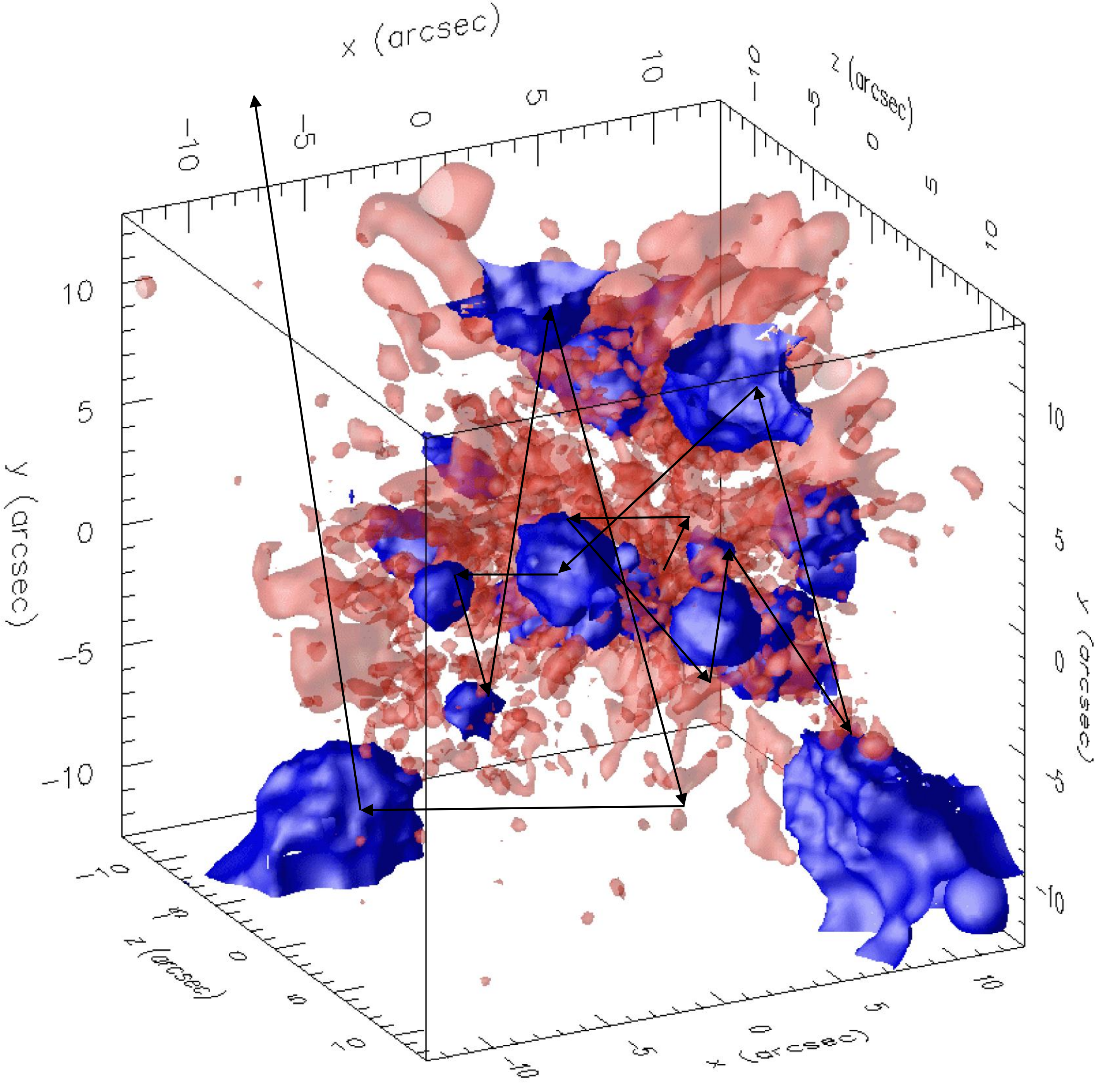

x (arcsec)
−10
−5
0
5
10
z (arcsec)
−10
−5
0
5
10
y (arcsec)
10
5
0
−5
−10
y (arcsec)
10
5
0
−5
−10
z (arcsec)
−10
−5
0
5
10
x (arcsec)
−10
−5
0
5
10

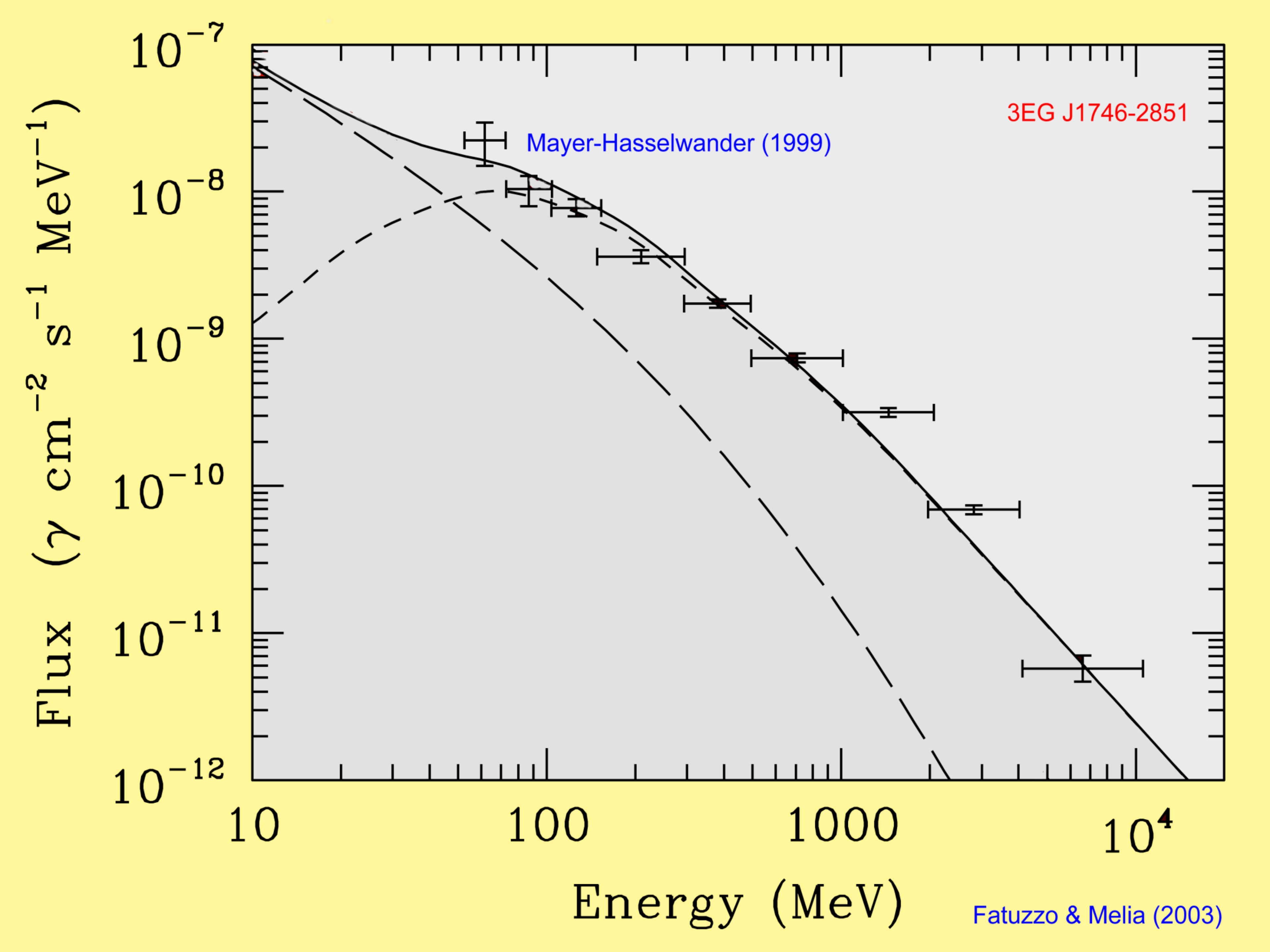

Flux (γ cm⁻² s⁻¹ MeV⁻¹)
Energy (MeV)
3EG J1746-2851
Mayer-Hasselwander (1999)
Fatuzzo & Melia (2003)

Active Galactic Nuclei

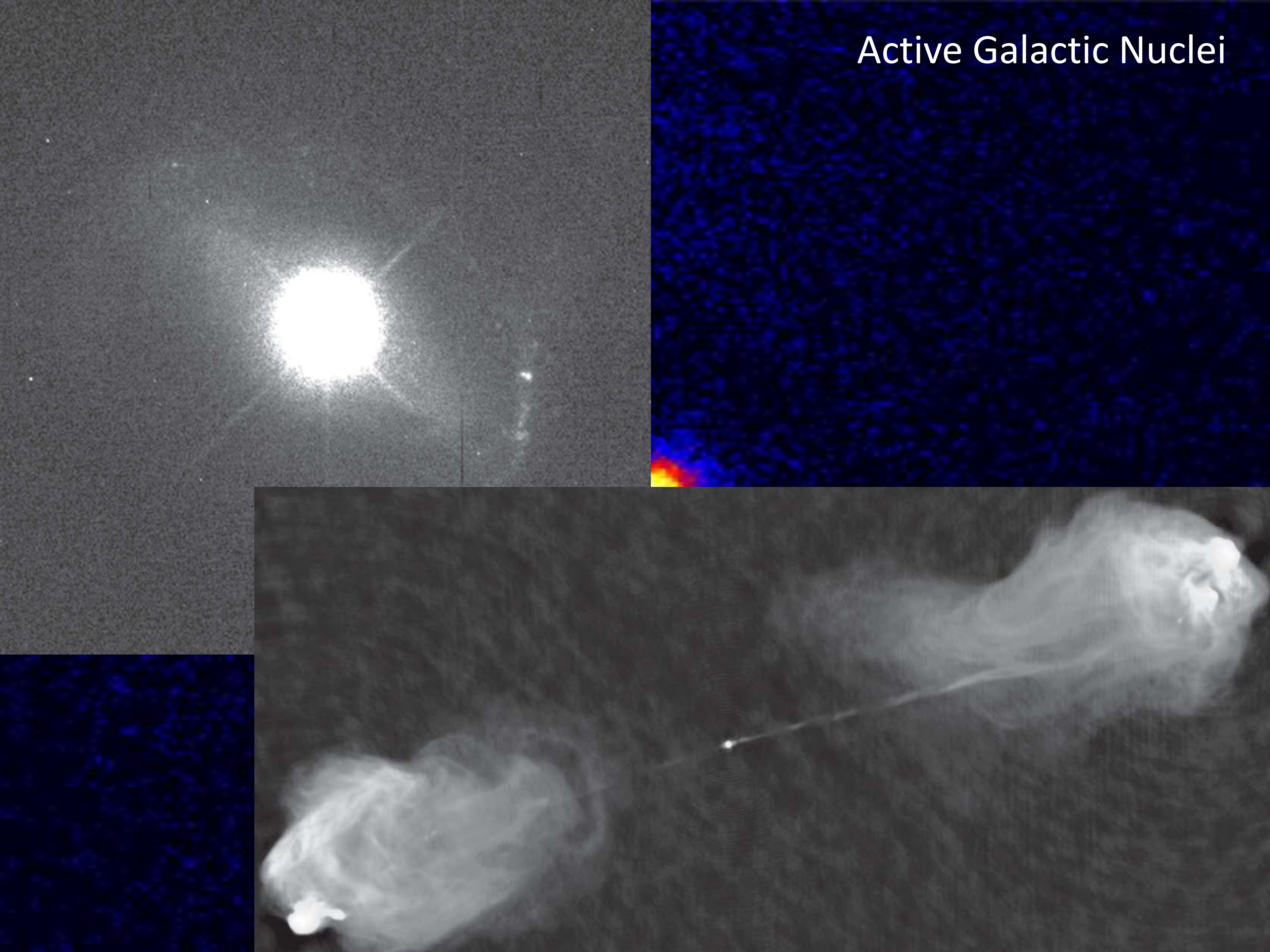

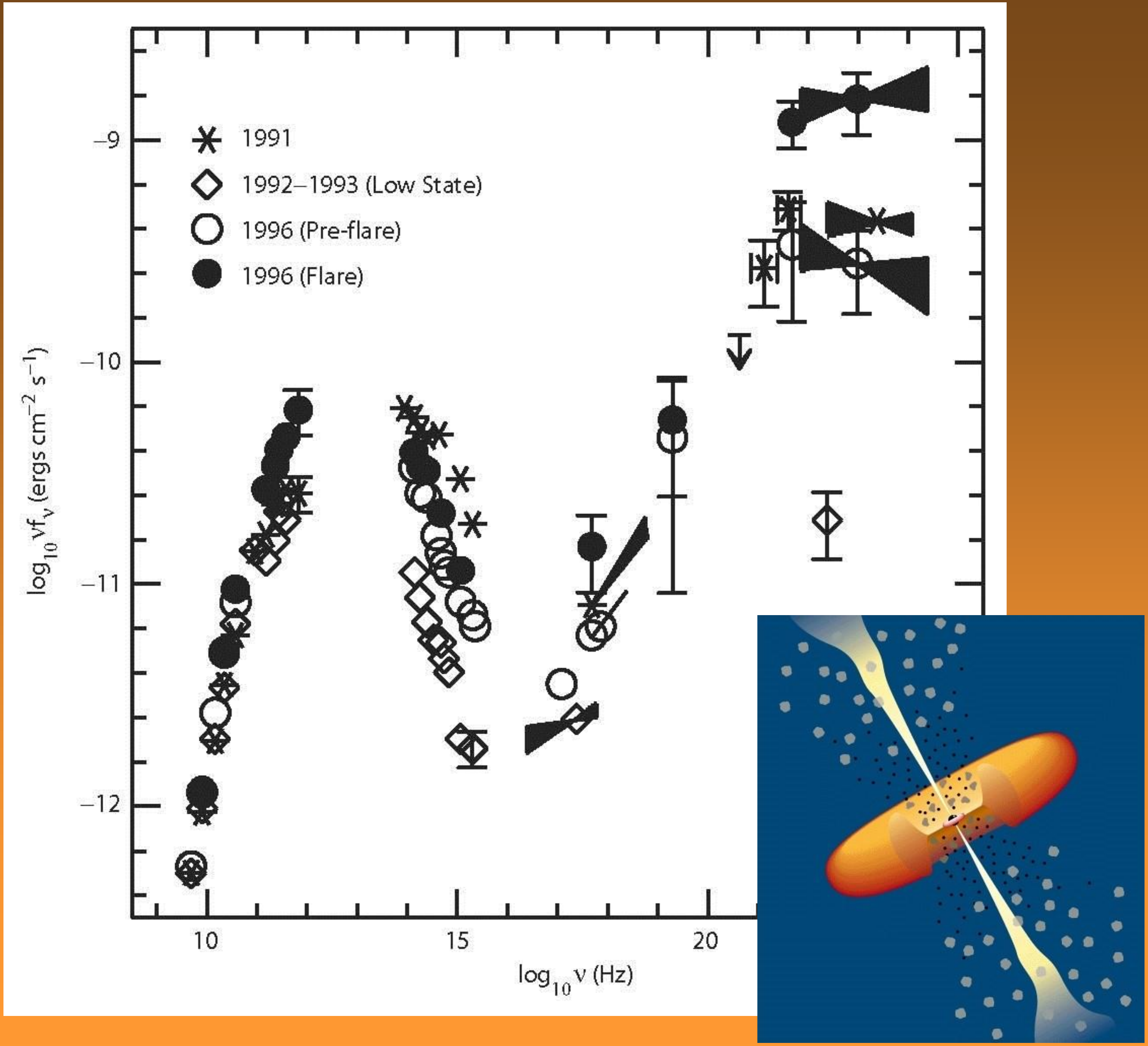

1991
1992–1993 (Low State)
1996 (Pre-flare)
1996 (Flare)
$\log_{10} \nu f_\nu$ (ergs cm^{-2} s^{-1})
$\log_{10} \nu$ (Hz)
–9
–10
–11
–12
10
15
20

FR I radio galaxy: *most of the energy comes from a small nucleus with weaker emission in a halo around the nucleus.*

Visible image of the core-halo (FR I) radio galaxy M87.

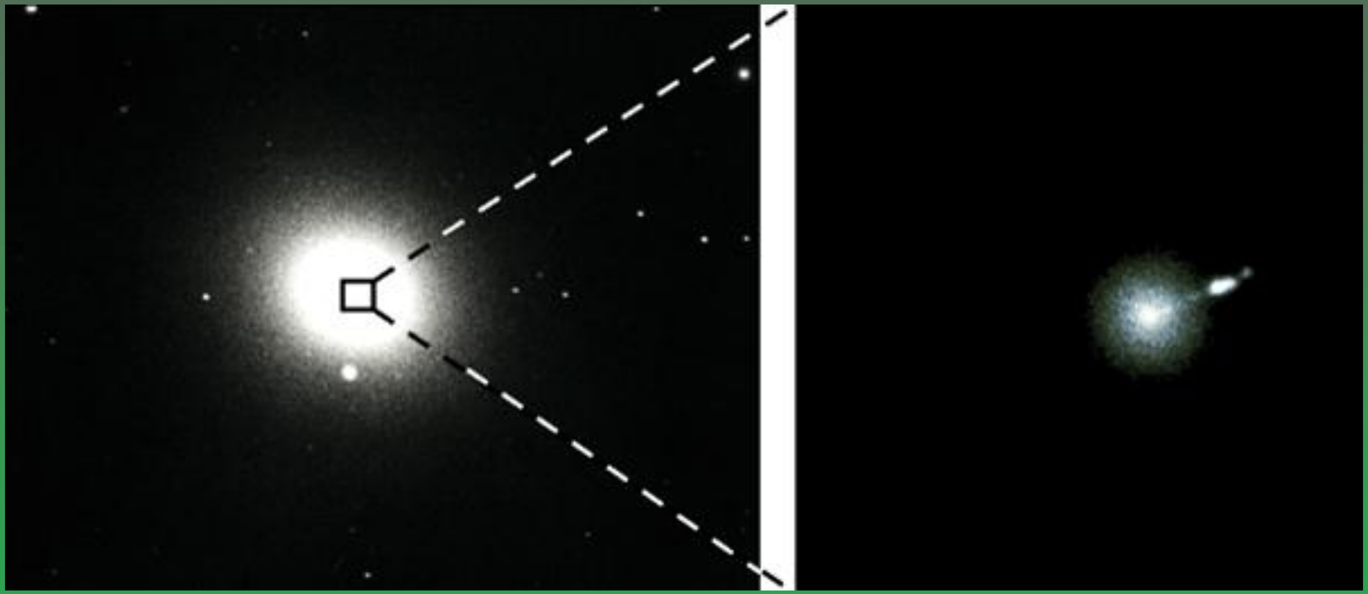

M87 is a giant elliptical (E1) galaxy ~100 Kpc across.

Jet was first noticed by Curtis (1918)

M87 was much later discovered to be a radio source

Jet in M87 at optical/radio wavelengths.

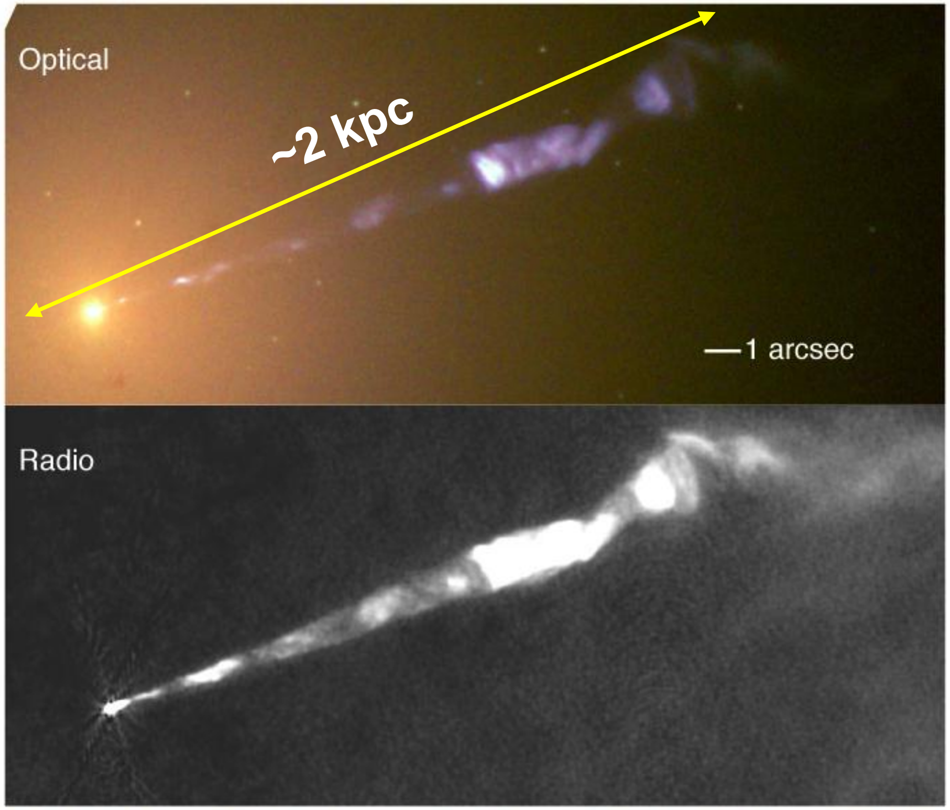

Fig 9.5 (J Biretta/HST) 'Galaxies in the Universe' Sparke/Gallagher CUP 2007

The jet is a series of distinct "blobs", ejected by the galaxy nucleus, and moving at up to half the speed of light.

Superluminal Motion

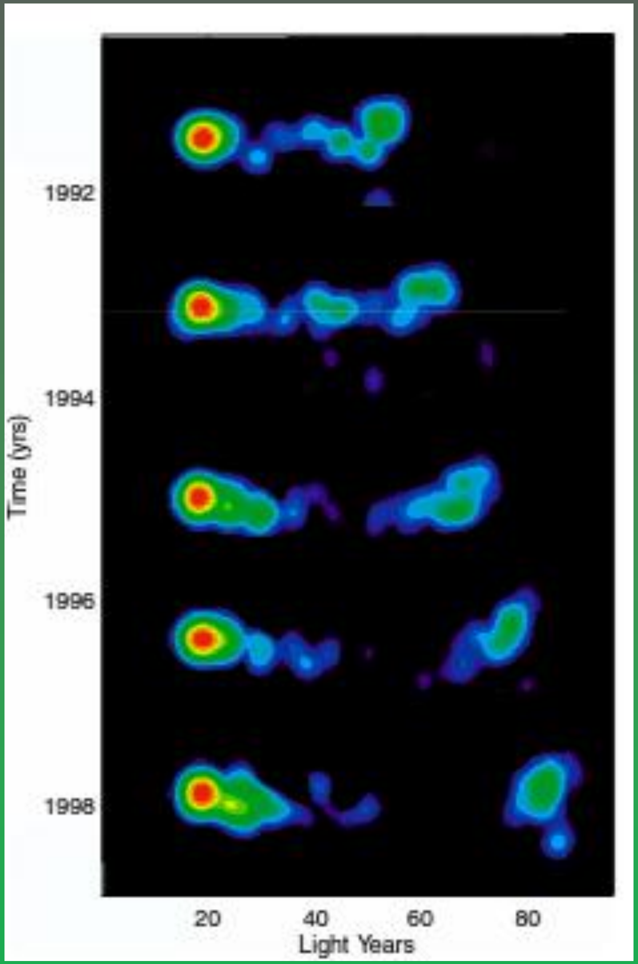

Some radio "blobs" in jets appear to move faster than c!

For object moving distance r below:
$x = r \cos \theta$, $y = r \sin \theta$ and $t = r/v$

Light from P takes x/c less time to reach us than light emitted from O.

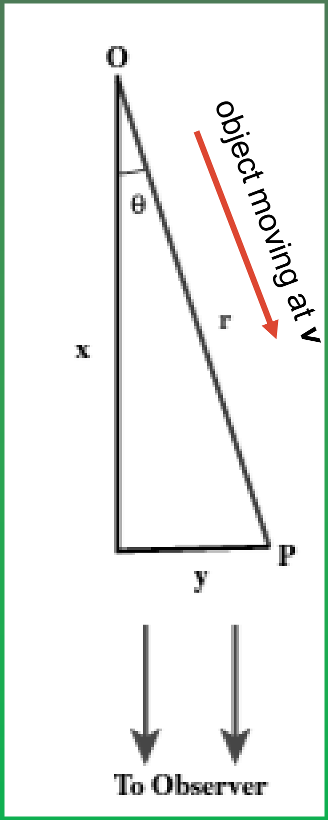

Time the observer sees for object to travel from O to P is

$t_{app} = t - x/c$

$t_{app} = (r/v) - (r/c) \cos \theta$

$t_{app} = (r/v) (1 - \beta \cos \theta)$

Apparent velocity across sky

$v_{app} = y/t_{app}$

$v_{app} = (v \sin \theta)/(1 - \beta \cos \theta)$

$v_{app} = (v \sin \theta)/(1 - \beta \cos \theta)$

For $v << c$, β is close to 0 and
$v_{app} = v \sin\theta$

For v close to c, v_{app} can be much more than v and even greater than c

Superluminal motion is observed in ~1/2 of well-studied cores

It occurs when $\theta \leq 10$ degrees

The jet appears brighter towards us due to relativistic boosting

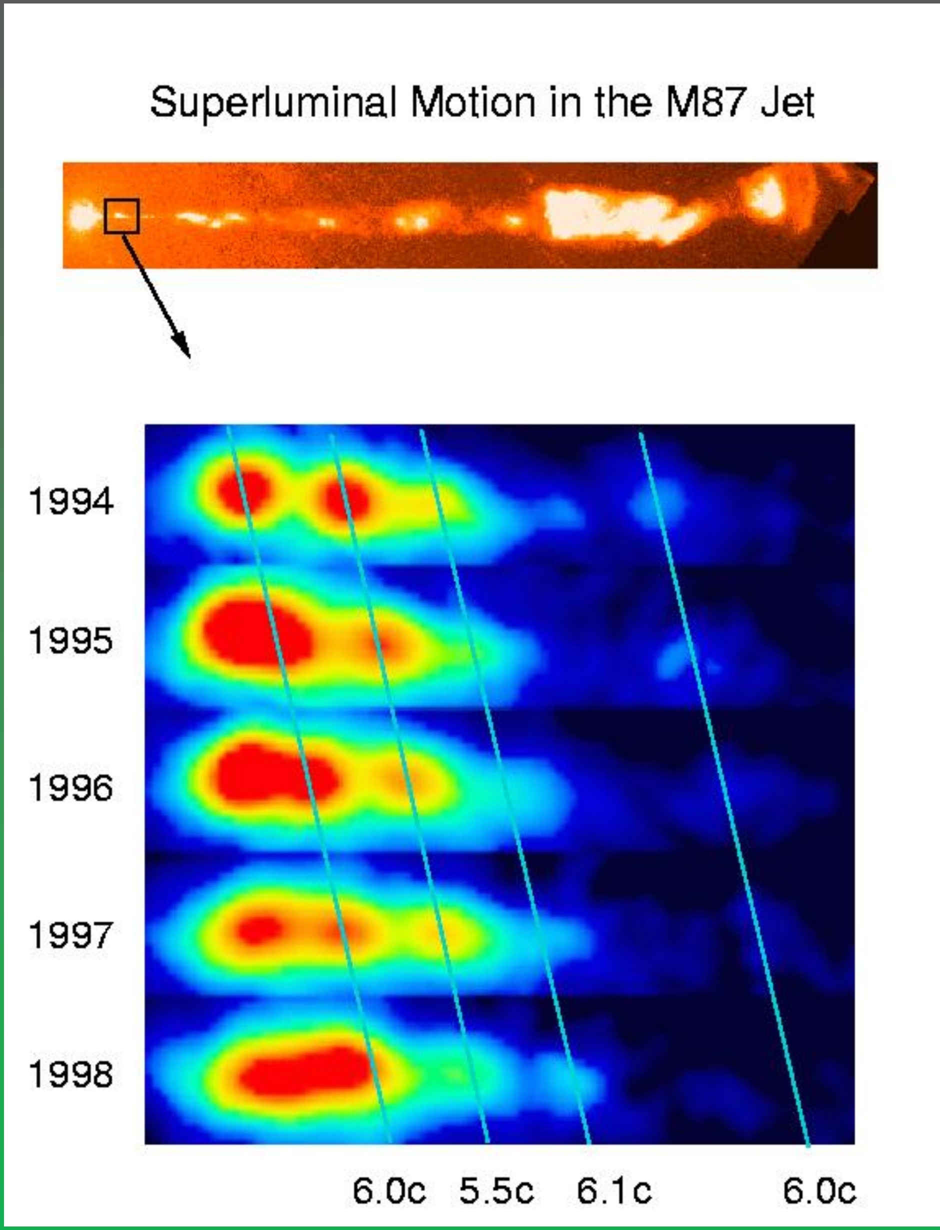

Black-Hole Imaging

Toward mm-submm wavelengths, the thin hot gas radiates predominantly via thermal synchrotron processes. Although the event horizon itself is not visible, the black hole's shadow appears as a depression in the line-of-sight emissivity. Light from the infalling gas behind Sgr A* does not make it directly to us because of strong gravitational bending, or simply absorption by the black hole. The shadow's size depends only weakly on the metric (though its shape can change), and has

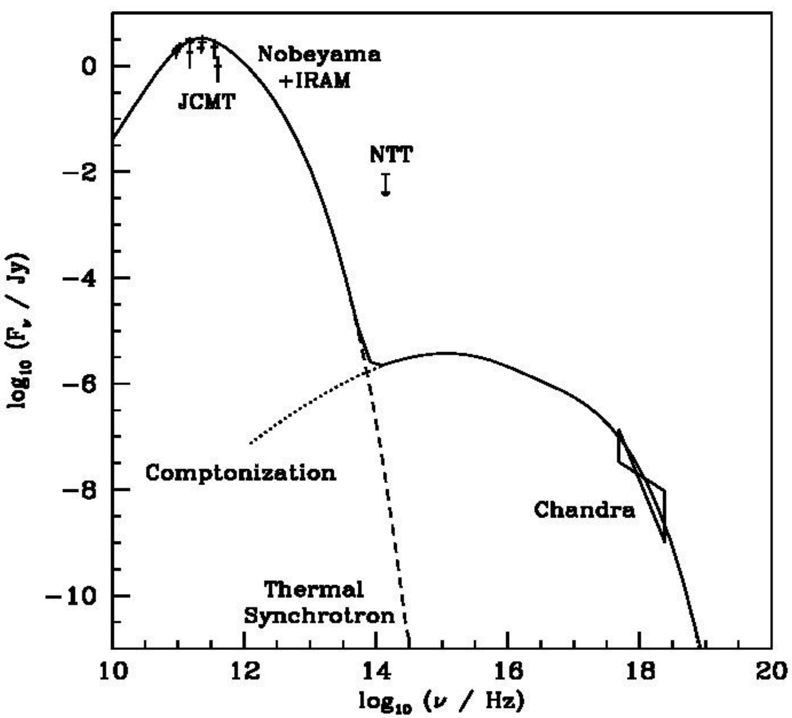

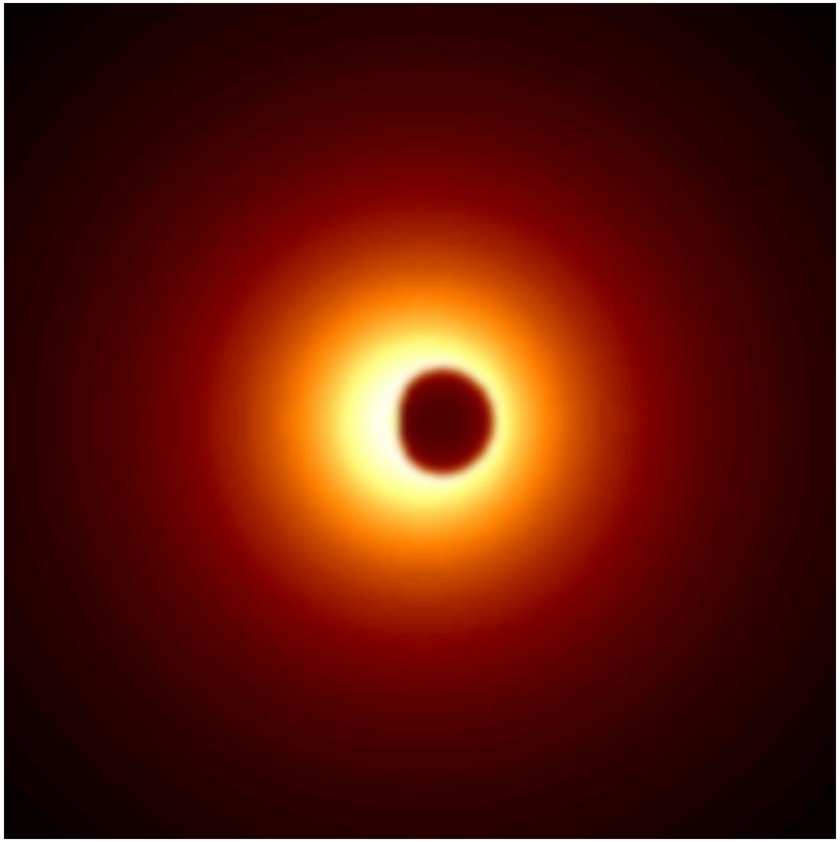

(with Falcke & Agol 2000)

a diameter of about 5 Schwarzschild radii. This image assumes no scattering by the intervening medium, and an ideal telescope resolution. At the distance to the Galactic center, this diameter corresponds to about 30 microarcseconds across.

Polarization

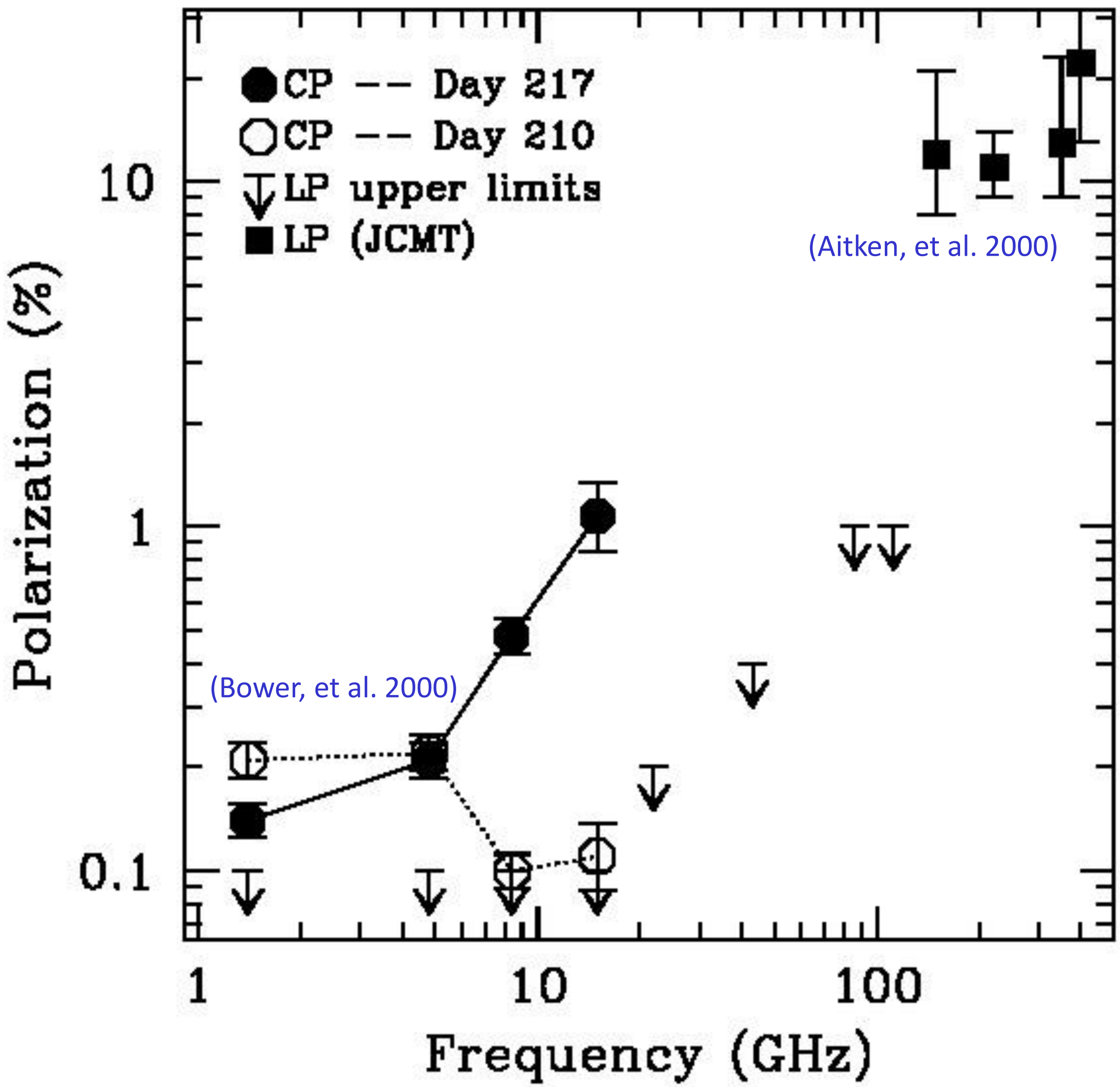

Polarization

The synchrotron emission is polarized because $B \approx B_\phi$ in the Keplerian region.

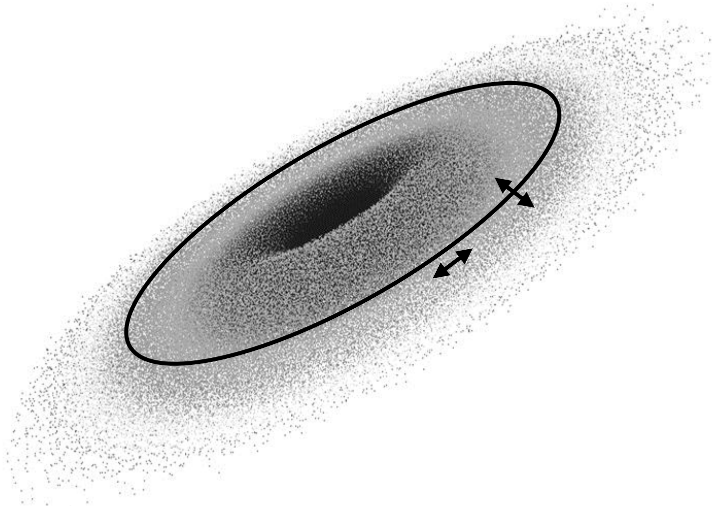

As the charges spiral around B, the extraordinary component is parallel to the disk's spin axis in front and behind the black hole, and perpendicular to it on the sides.

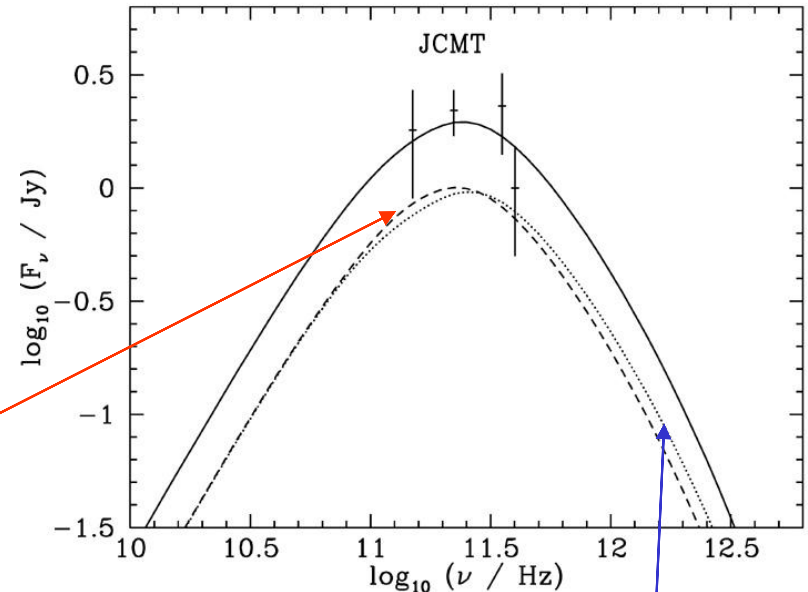

The ordinary component does the opposite. But the medium goes from optically thick to thin across $2-3\times10^{11}$ Hz, so the net polarization vector flips by 90 degrees (from vertical to horizontal) near the peak of the mm-hump.

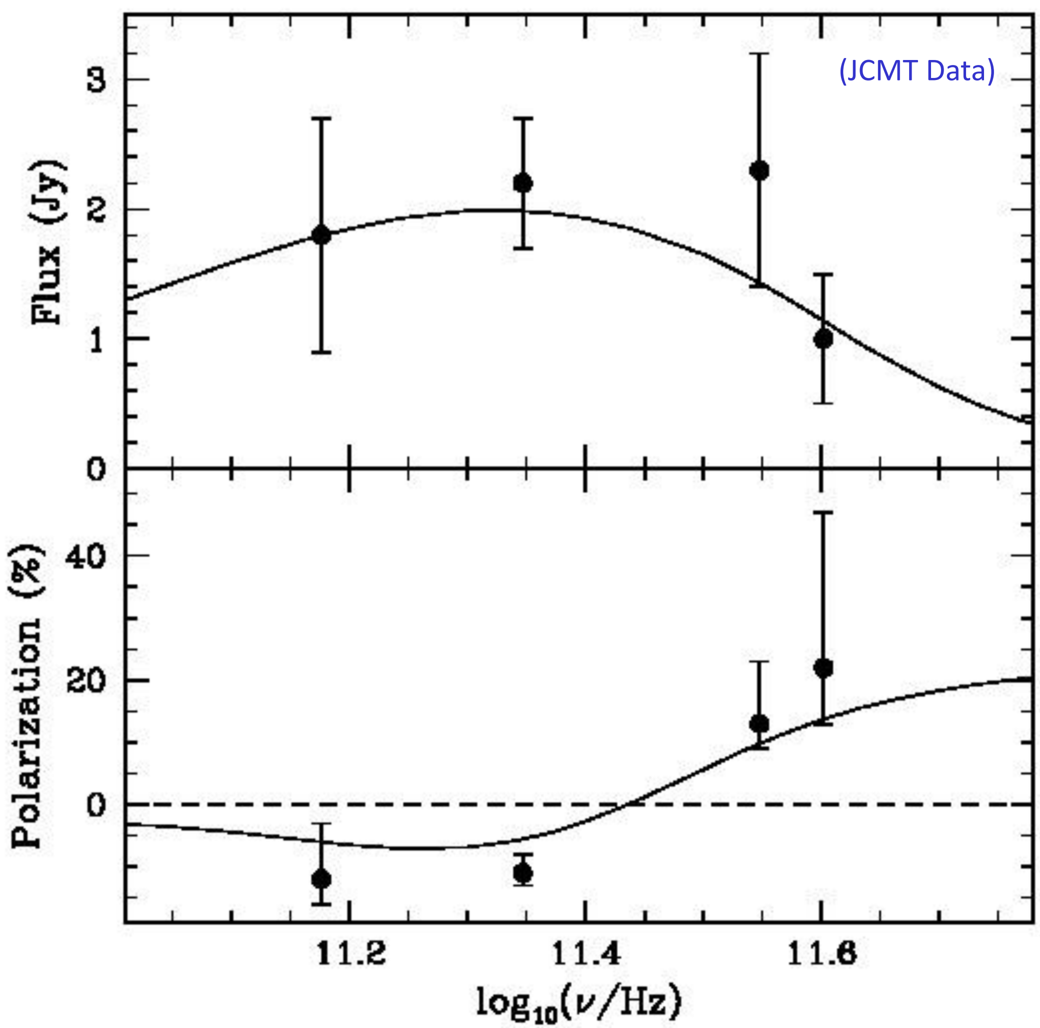

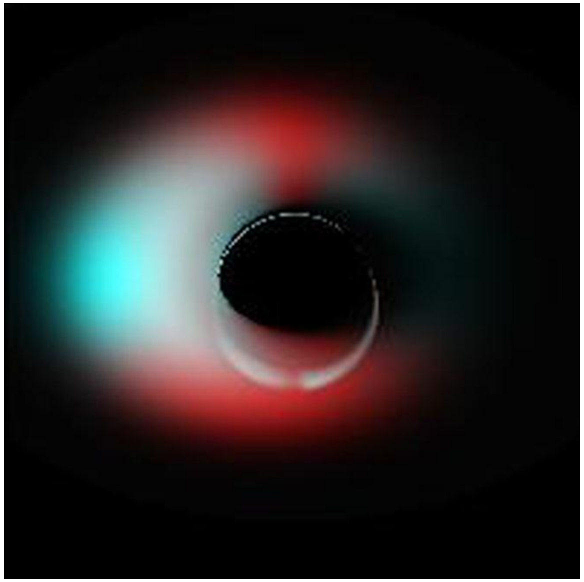

Image of 1.5 mm emission, dominated by the circularized flow within 10 Schwarzschild radii of the black hole.

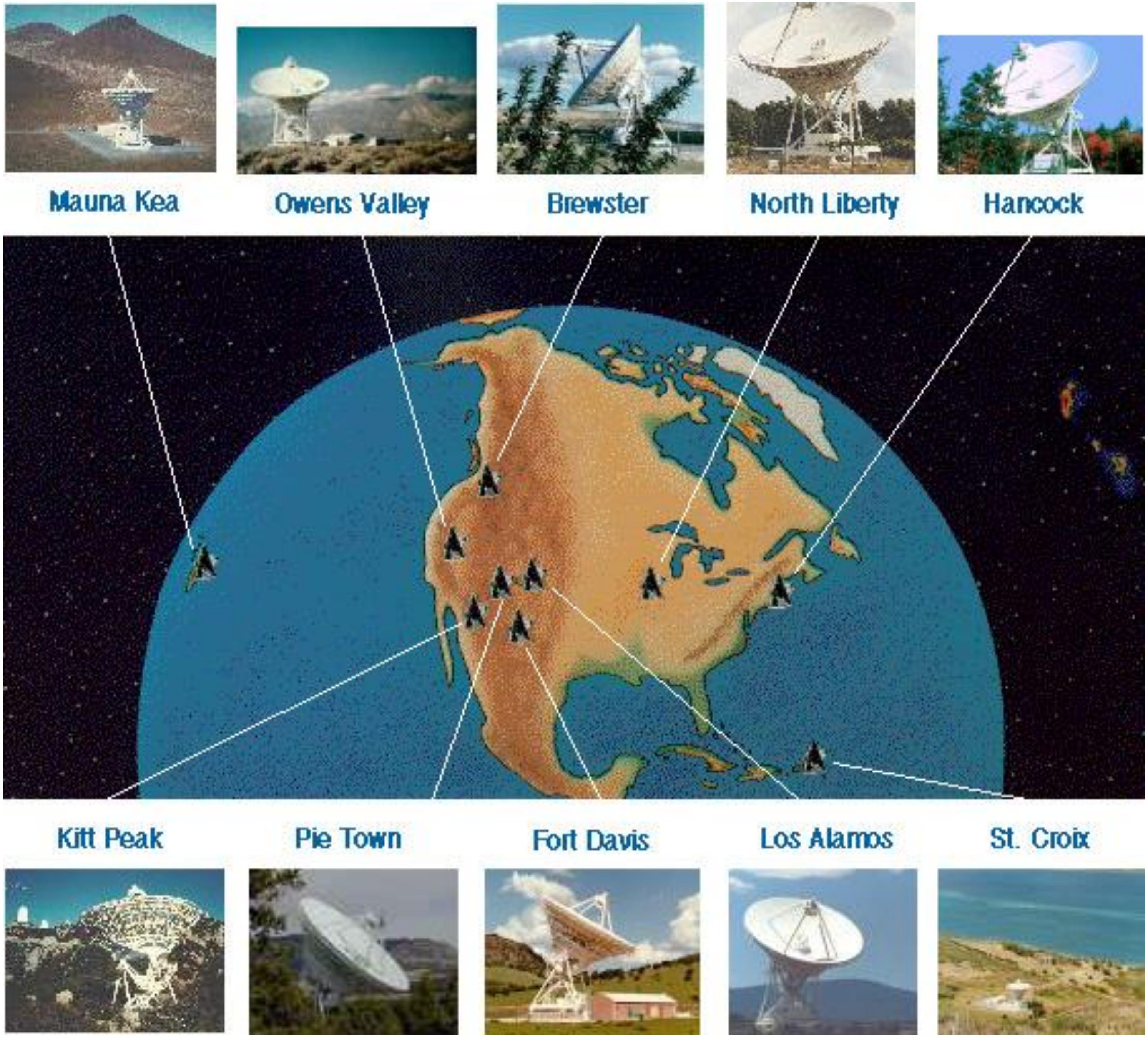
Mauna Kea
Owens Valley
Brewster
North Liberty
Hancock
Kitt Peak
Pie Town
Fort Davis
Los Alamos
St. Croix

Polarimetric Imaging with Sub-mm VLBI

The predicted size (~30 microarcsecs) of the mm-emitting region approaches the resolution of current radio interferometers. However, there are still too few single-dish telescopes that can operate at mm and sub-mm wavelengths.

In addition, there are two complications that really force the optimum imaging region to lie at or below ~0.7 mm:

[1] scatter-broadening of the image by the ISM. This is incorporated by smoothing the image with an elliptical Gaussian with a FWHM of

$24.2 \text{ mas} \times (\lambda / 1.3 \text{ mm})^2$ along the major axis and

$12.8 \text{ mas} \times (\lambda / 1.3 \text{ mm})^2$ along the minor axis (Lo et al. 1998).

[2] the finite achievable telescope resolution from the ground. This is added by convolving the smoothed image with a spherical Gaussian point-spread function of FWHM

$$33.5 \text{ mas} \times (\lambda / 1.3 \text{ mm})\,(L / 8{,}000 \text{ km})^{-1}$$

for an idealized global interferometer (Krichbaum 1996).

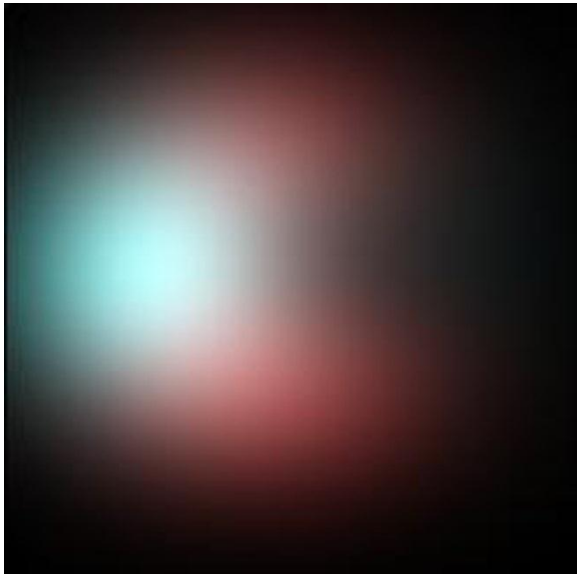

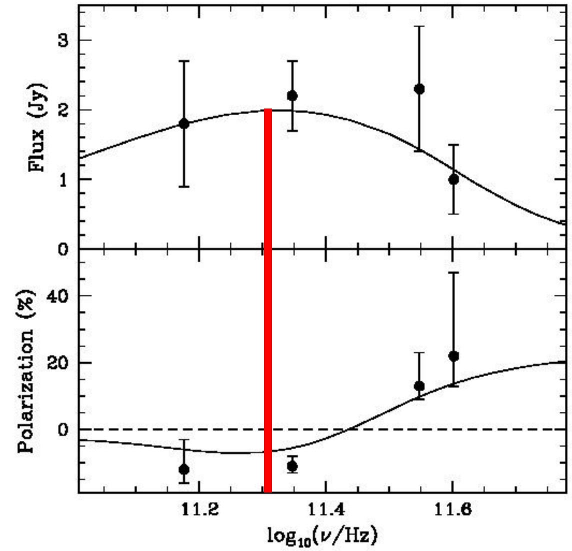
Flux (Jy)
Polarization (%)
$\log_{10}(\nu/\mathrm{Hz})$
0
1
2
3
0
20
40
11.2
11.4
11.6

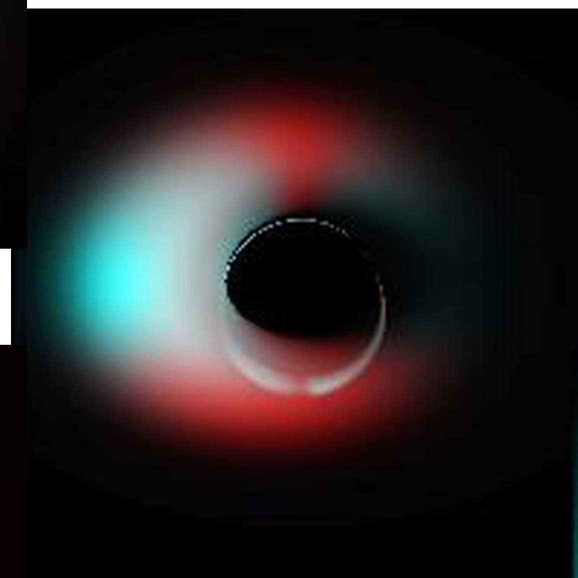

1.5 mm

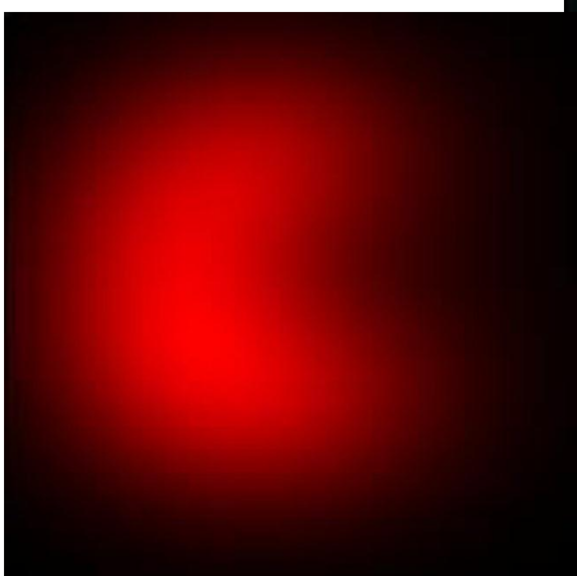

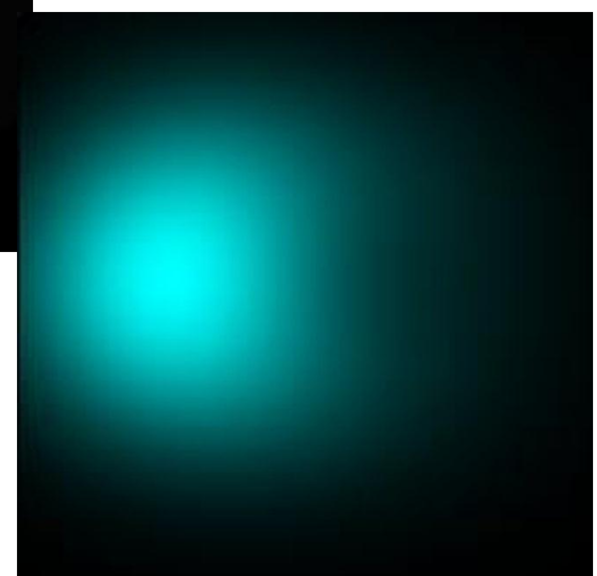

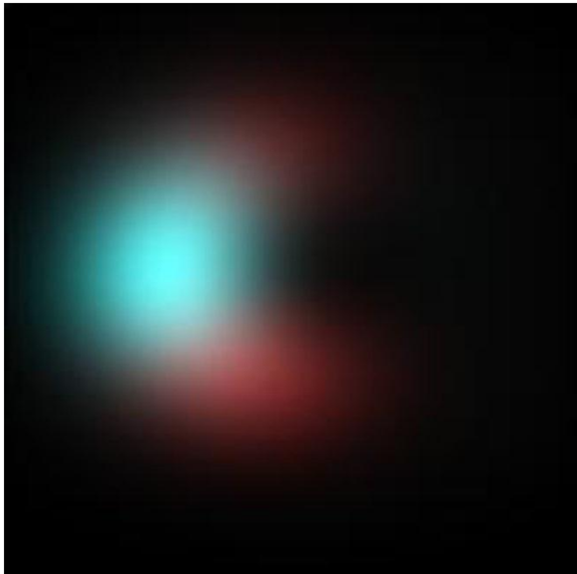

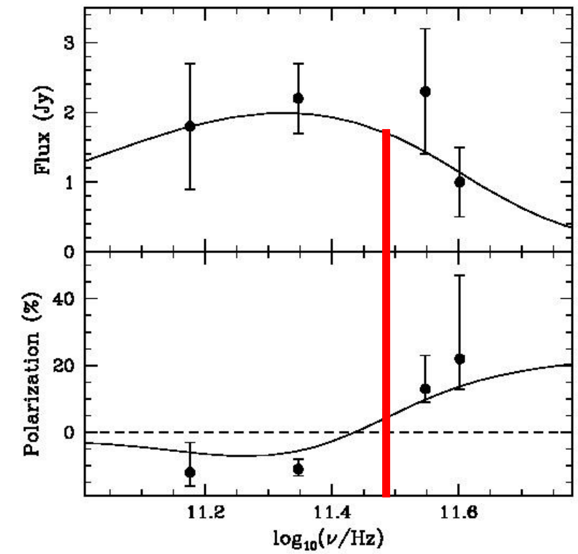
Flux (Jy)
Polarization (%)
$\log_{10}(\nu/\mathrm{Hz})$
11.2
11.4
11.6
0
1
2
3
0
20
40

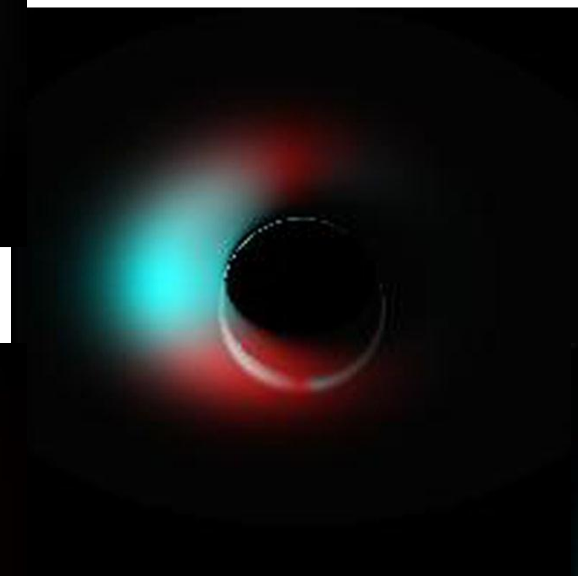

1 mm

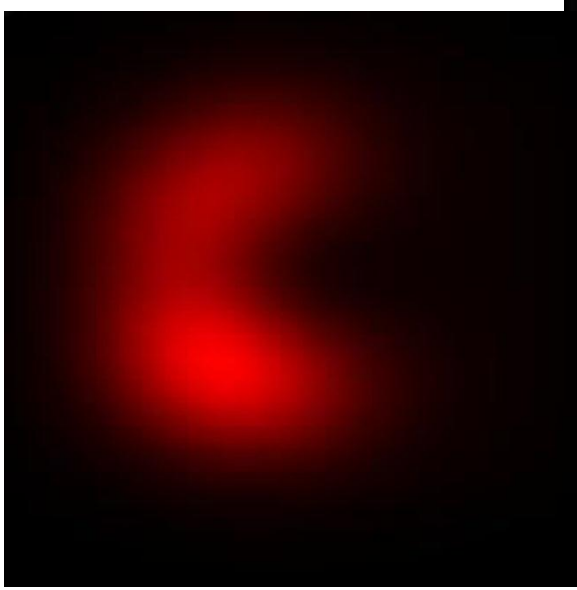

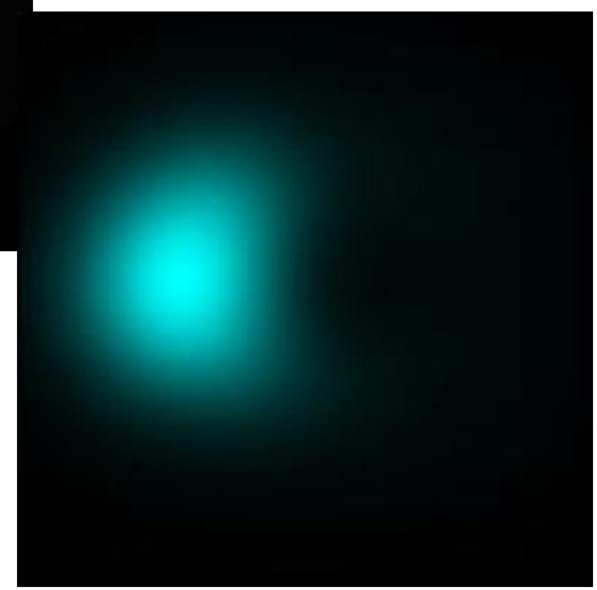

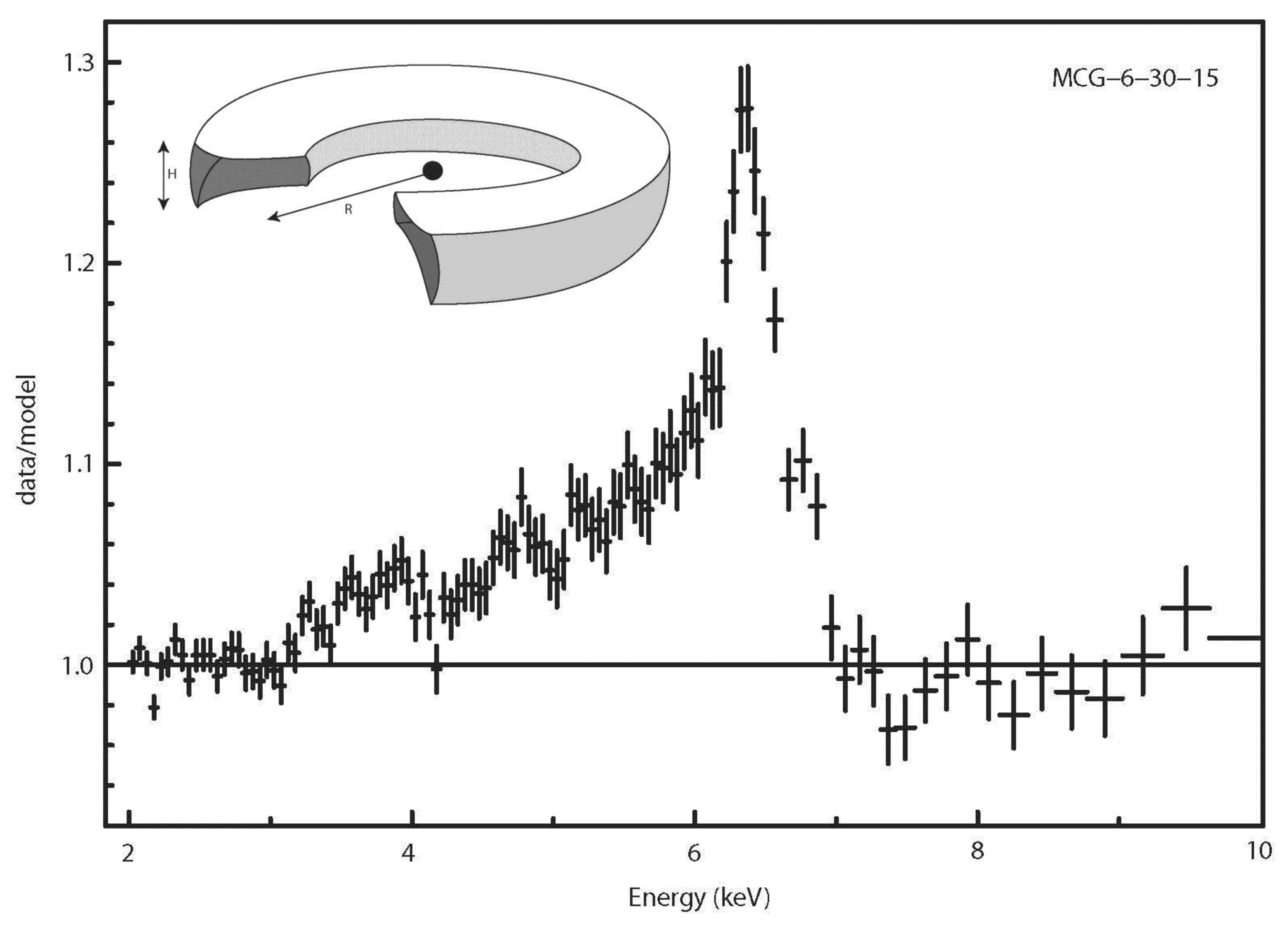
MCG–6–30–15
H
R
1.3
1.2
1.1
1.0
data/model
2
4
6
8
10
Energy (keV)

Mass Transfer and Accretion in Binaries

$$\vec{a}_1 = -\frac{GM_1}{|\vec{r}-\vec{r}_1|}(\vec{r}-\vec{r}_1) \qquad \vec{a} = -\vec{\nabla}\Phi_R$$

$$\vec{a}_2 = -\frac{GM_2}{|\vec{r}-\vec{r}_2|}(\vec{r}-\vec{r}_2) \qquad \Phi_R = -\frac{GM_1}{|\vec{r}-\vec{r}_1|} - \frac{GM_2}{|\vec{r}-\vec{r}_2|} - \frac{1}{2}(\vec{\omega}\times\vec{r})^2$$

$$\vec{a}_f = -\vec{\omega}\times(\vec{\omega}\times\vec{r})$$

$$v_\varphi(R_{circ}) = \left(\frac{GM_1}{R_{circ}}\right)^{1/2}$$

$$R_{circ}v_\varphi(R_{circ}) = b_{L1}{}^2\omega$$

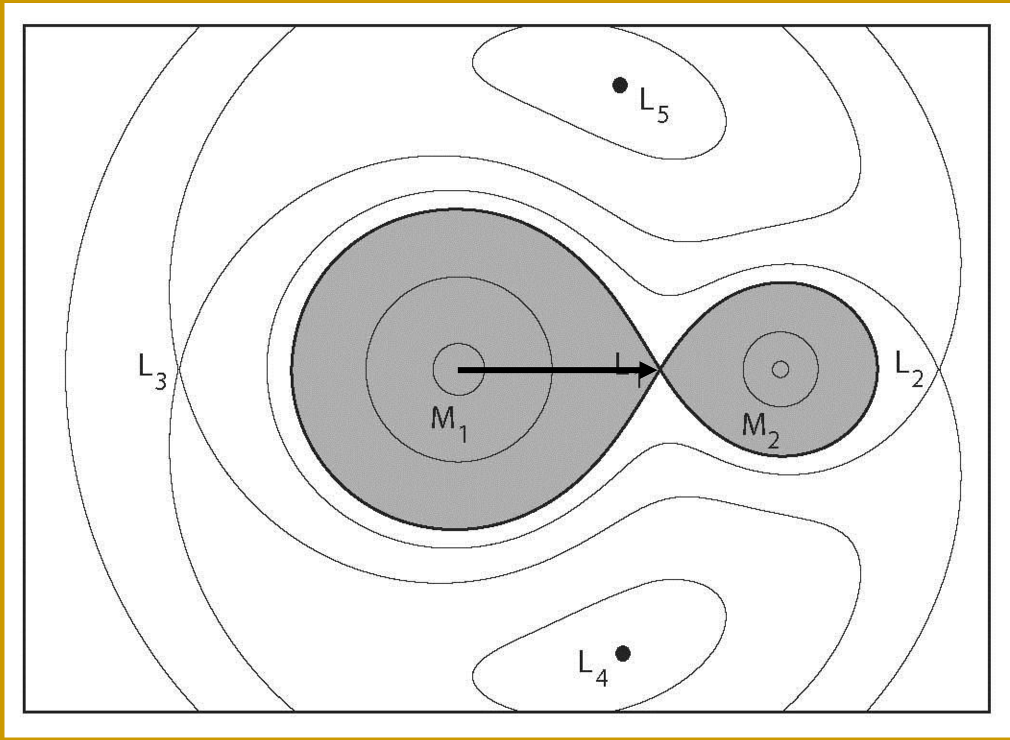

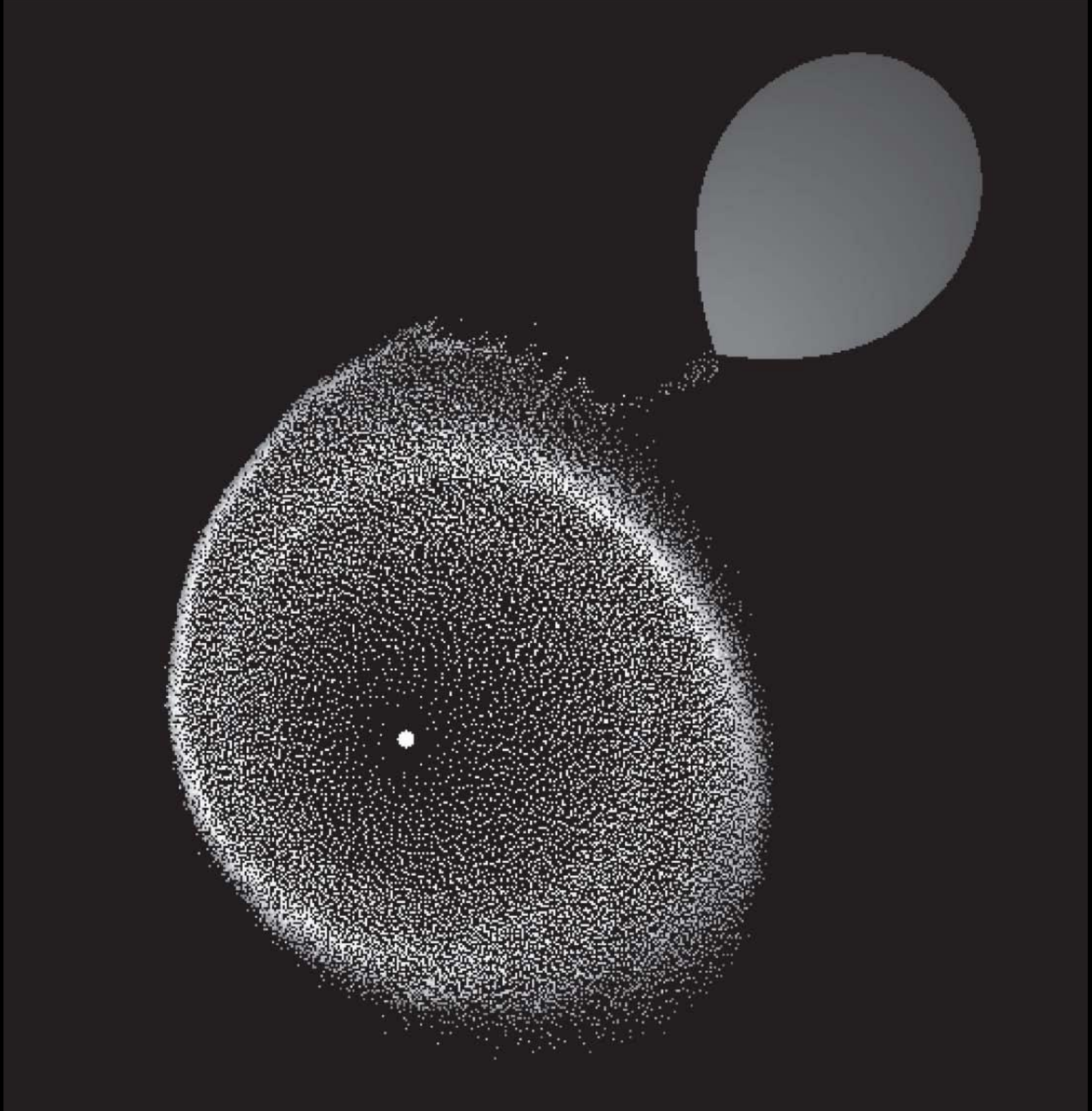

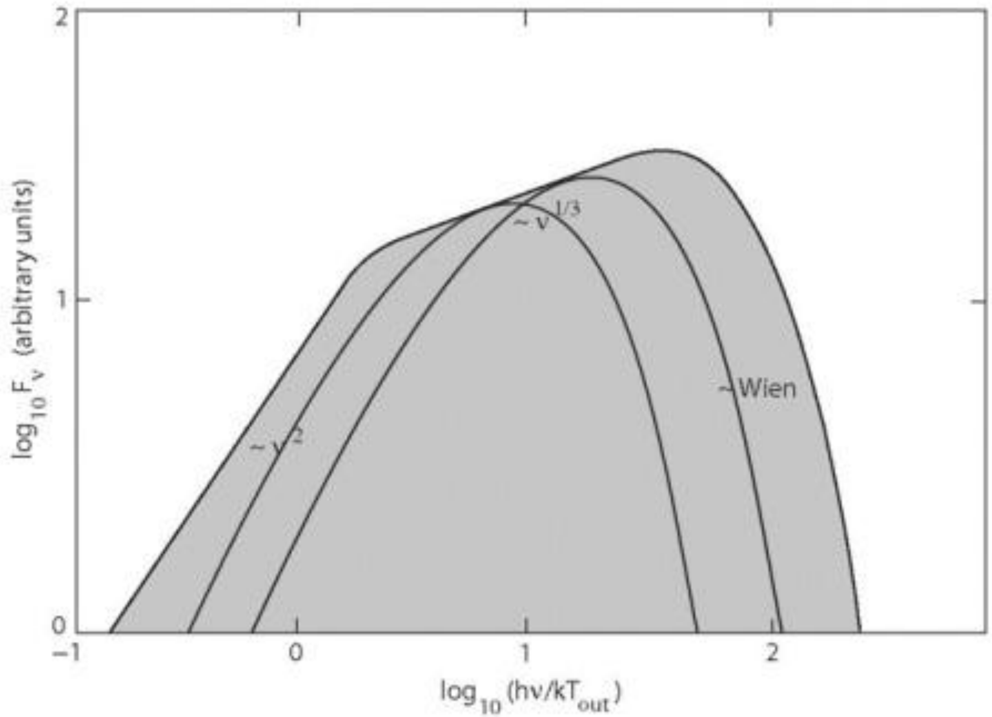

2
1
0
−1
0
1
2
$\log_{10} F_\nu$ (arbitrary units)
$\log_{10}(h\nu/kT_{out})$
$\sim \nu^2$
$\sim \nu^{1/3}$
~Wien

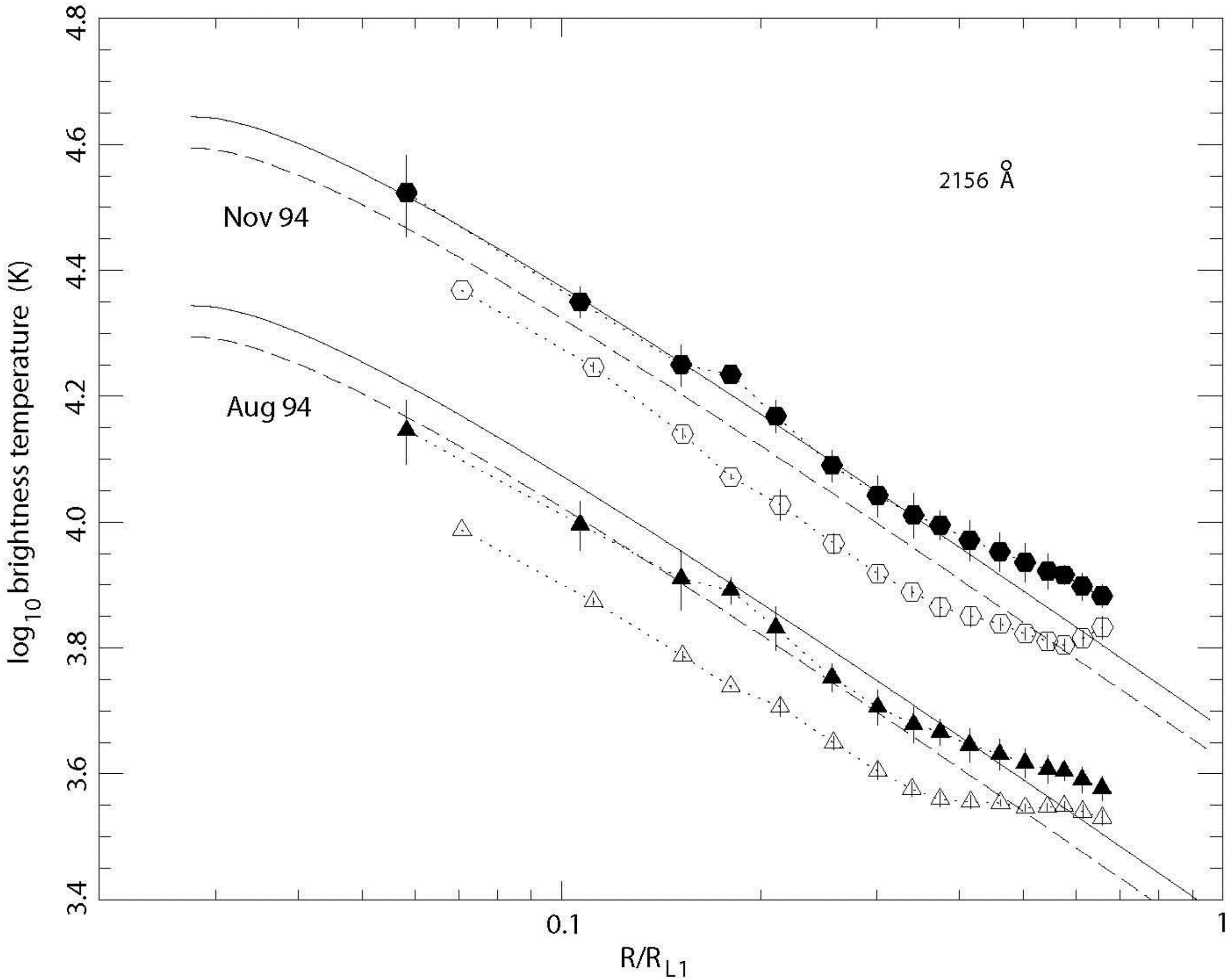

4.8
4.6
4.4
4.2
4.0
3.8
3.6
3.4
$\log_{10}$brightness temperature (K)
2156 Å
Nov 94
Aug 94
0.1
1
R/R_{L1}

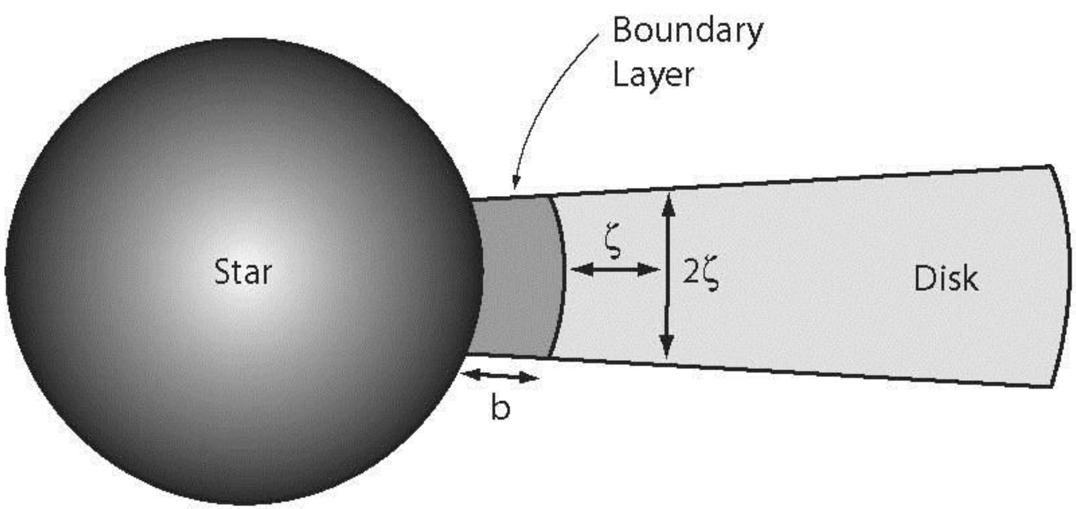

$$\frac{v^2}{R} = \frac{GM}{R^2} \rightarrow v_K = \sqrt{\frac{GM}{R}}$$

$$\frac{1}{2}v^2 = \frac{GM}{R} \rightarrow v_{esc} = \sqrt{\frac{2GM}{R}}$$

$$v_K = \frac{1}{\sqrt{2}}v_{esc} \rightarrow \boxed{E(R_*) = \frac{1}{2}{v_K}^2 = \frac{1}{2}E(R_{out})}$$

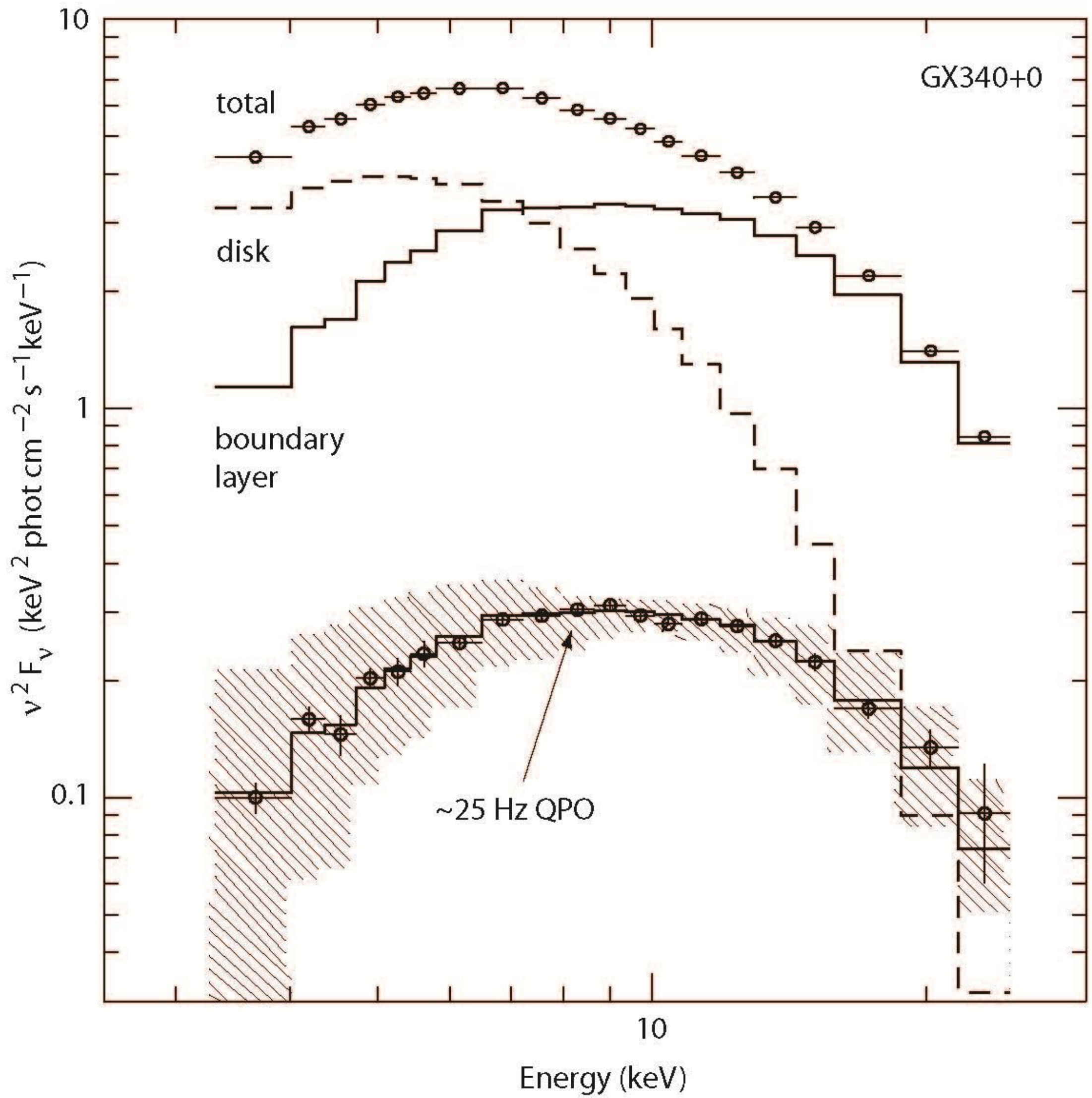

GX340+0
total
disk
boundary
layer
~25 Hz QPO
10
1
0.1
10
Energy (keV)
$\nu^2 F_\nu$ (keV^2 phot cm^{-2} s^{-1}keV^{-1})

X-ray Bursters

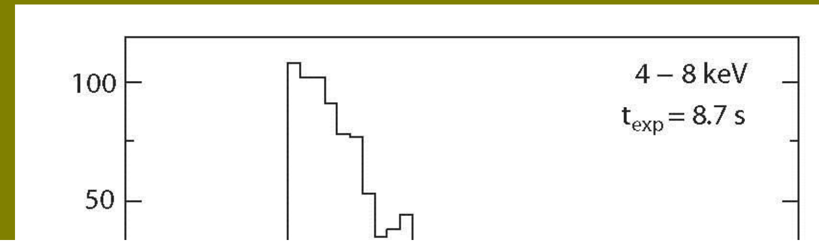

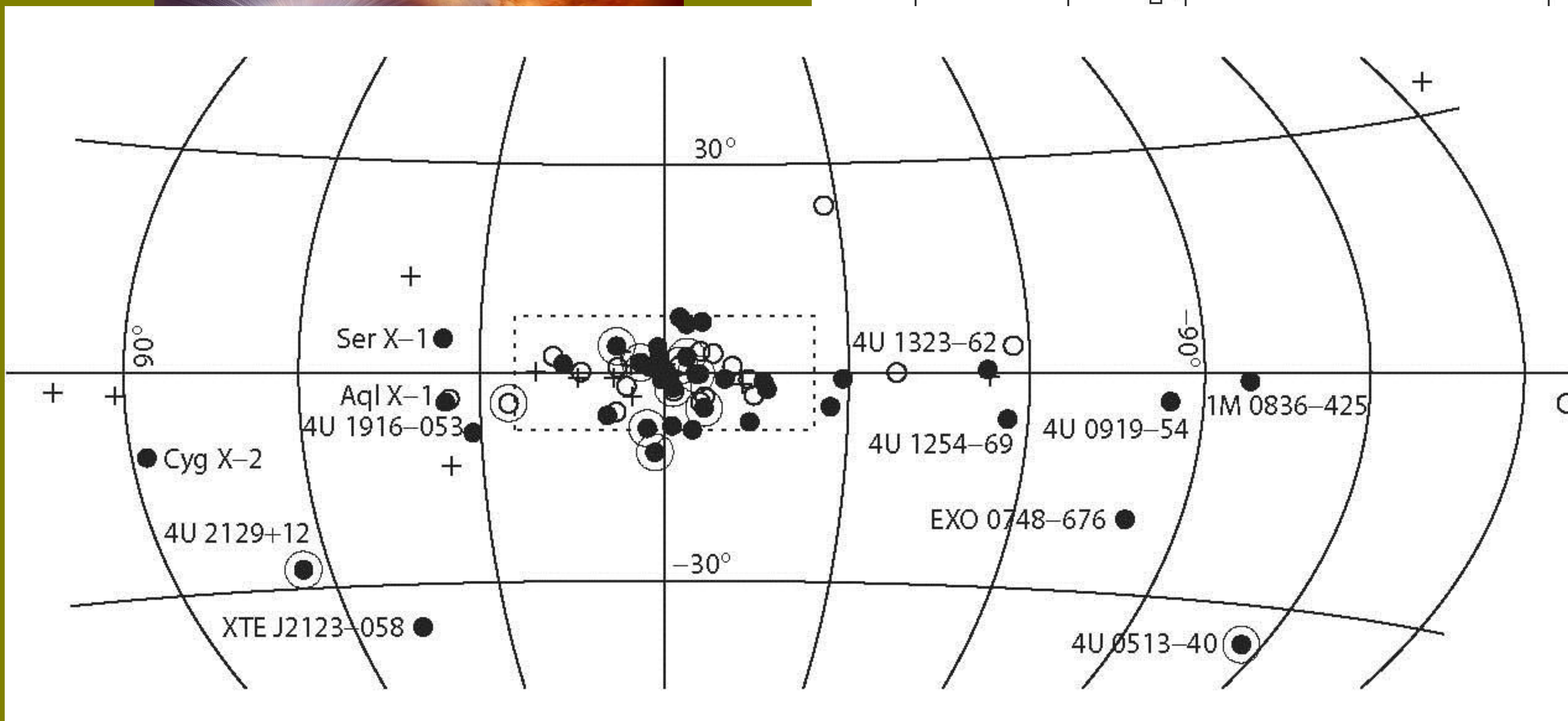

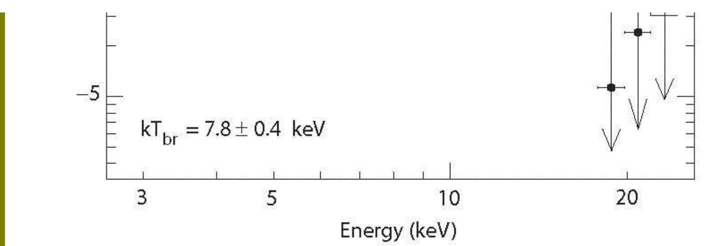

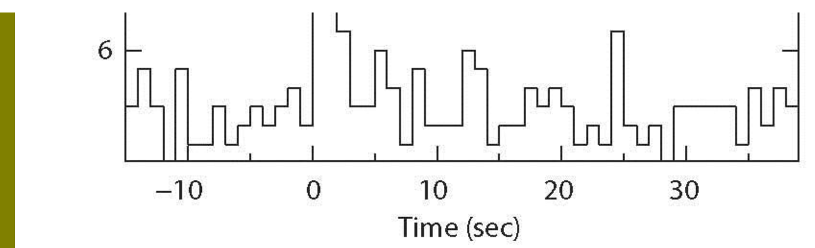

X-ray Bursters